InterPore JOURNAL

Special Issue – Iran 2024
Original Research

PARETO-BASED MULTI-OBJECTIVE OPTIMIZATION OF UNDERGROUND HYDROGEN STORAGE OPERATIONAL CONDITION UTILIZING MACHINE LEARNING-BASED SURROGATE MODELS

Hossein Kheirollahi, Shahab Ayatollahi, Hassan Mahani

Sharif University of Technology, Department of Chemical and Petroleum Engineering, Tehran, Iran

Correspondence to:
Hassan Mahani,
hmahani@sharif.edu

How to Cite:
Kheirollahi, H., Ayatollahi, S., & Mahani, H. (2026). Pareto-based Multi-Objective Optimization of Underground Hydrogen Storage Operational Condition Utilizing Machine Learning-Based Surrogate Models. *InterPore Journal*, *3*(1), IPJ010326-6. https://doi.org/10.69631/m0g16y60

RECEIVED: 2 Oct. 2025
ACCEPTED: 8 Jan. 2026
PUBLISHED: 1 Mar. 2026

ABSTRACT

Underground hydrogen storage (UHS) in depleted hydrocarbon reservoirs, saline aquifers, and salt caverns has emerged as a promising solution for large-scale, long-term energy storage to support the energy transition. However, evaluating the feasibility of UHS requires addressing substantial uncertainties in geological, operational, and economic factors. Physics-based reservoir simulations, though accurate, are computationally expensive and impractical for exploring a wide range of operational scenarios and optimization problems. To overcome these challenges, this study employs an intelligent surrogate model constructed using data collected from Latin hypercube sampling and validated against detailed reservoir simulations to perform sensitivity analysis and formulate a multi-objective optimization framework. The primary objectives are to maximize hydrogen recovery factor and hydrogen purity in the produced gas, while also incorporating net present value (NPV) as an economic criterion. Multi-objective optimization is performed using the Non-dominated Sorting Genetic Algorithm II (NSGA-II), which enables efficient exploration of the trade-offs between conflicting objectives and provides a Pareto front of non-dominated solutions. This Pareto-based decision-making framework offers valuable insights into selecting optimal storage strategies under uncertainty. The results highlight two key findings. First, pure nitrogen (N_2) as a cushion gas yields higher hydrogen mole fraction in production stream compared to CO_2 and CH_4, because of favorable segregation and flow behavior in porous media. Second, the optimal cushion gas mixture was determined to be 45% N_2, 40% CO_2, and 15% CH_4, balancing recovery and purity objectives. Nevertheless, from both economic and operational efficiency perspectives, a CO_2 fraction of 100%

emerges as the optimal solution. Additionally, injecting from bottom perforations and producing from top perforations was identified as the most effective configuration due to the gravity override effect of hydrogen. Importantly, re-simulation of the Pareto-optimal solutions confirmed the robustness and reliability of the surrogate-based optimization approach. This study demonstrates the capability of coupling surrogate modeling with evolutionary multi-objective optimization to design cushion gas, optimize injection/withdrawal schemes, and maximize both technical and economic performance of large-scale underground hydrogen storage projects.

KEYWORDS
Underground hydrogen storage, Depleted gas reservoirs, Machine learning, Surrogate models, Genetic algorithms, Energy transition

1. INTRODUCTION

Anthropogenic greenhouse gas emissions (e.g., carbon dioxide) from fossil fuel consumption are the primary drivers of the greenhouse effect and global warming in the current era. However, population growth and the continuing rise in carbon dioxide emissions have compelled the global economy to seek solutions to mitigate these emissions and their adverse consequences, including global warming, climate change, polar ice melt, and rising sea levels (12, 24).

Over the past years, several studies have been conducted on near- and net-zero carbon strategies and energy-transition pathways toward a hydrogen economy to address these challenges and fulfill increasing energy demand. In this regard, most of the published articles have concentrated on investigating the large-scale and long-term feasibility of hydrogen storage as an energy carrier in subsurface depleted hydrocarbon reservoirs, saline aquifers and salt/man-made caverns, and the challenges associated with simulation and real-case implementation (4, 13, 15, 29). Time-intensive and costly physics-based full compositional simulation of underground hydrogen storage (UHS) and assessment of different scenarios have led to a growing focus on the development of proxy models, i.e., mathematical, or statistical models to replicate reservoir multiphase-flow simulation results. These models have been employed in synthetic or real field cases to address subsurface engineering practices (e.g., production optimization or forecasting) (5, 11, 19, 21, 25).

A number of recent studies highlight the variety of machine-learning architectures and reduced-order frameworks applied to UHS. Mao et al. (18) demonstrated that deep-neural-network-based reduced-order models can predict key performance indicators, such as hydrogen recovery and purity, with excellent accuracy and vastly reduced runtime. Similarly, Malki et al. (17) integrated surrogate models into the OPERATE-H_2 decision support tool, enabling practitioners to perform scenario testing and operational planning without repeated full-physics simulations. More advanced architectures have also been explored. Fu et al. (9) proposed a Swin-UNet transformer surrogate to forecast spatiotemporal hydrogen saturation and pressure fields in heterogeneous reservoirs, while Asghari et al. (2) introduced UHSNet, a Res-U-Net–based framework that achieved more than a 100-fold acceleration over computational fluid dynamics benchmarks. These examples illustrate how proxy models can transform simulation workflows by extending feasibility from academic demonstrations to practical decision-making.

Beyond fast simulation capabilities, proxy models have also been deployed for optimization and risk assessment in UHS. Han et al. (10) coupled a CNN–LSTM–Attention surrogate with a robust optimization framework to identify operational strategies that remain effective under geological uncertainty, while Esfandi et al. (7) used an XGBoost surrogate to analyze the influence of injection rate, cushion-gas composition, and fracture density on storage performance. Omeke et al. (22) developed hybrid Fourier-neural models to better capture sharp displacement fronts.

Although these approaches show remarkable potential, limitations remain, including reliance on synthetic training datasets, limited generalization to unseen geological settings, and the absence of large-scale field validation. Nevertheless, the convergence of reservoir engineering and

Table 1: Proxy/surrogate model applications in underground gas storage.

Authors	Storage gas	Reservoir type	Key finding(s)	Limitations
Matthew et al. (19)	CO_2 EOR	Oil reservoirs (synthetic Egg model & Gullfaks field model)	ML proxy models enabled fast multi-objective optimization of CO_2-WAG; best oil recovery at high gas-rate / low water-rate settings, but this reduces net CO_2 stored—highlighting recovery–storage trade-offs. Average proxy error <2% vs. simulator on tested cases.	Proxies are case-specific and trained on field-scale outputs; they cannot predict grid/well-scale states and may not generalize to other reservoirs without re-training.
Eltahan et al. (6)	H_2	Brugge benchmark field	Deep-learning-accelerated gradient (DLAG) method sped convergence and improved optimized well placements for H_2 storage deliverability; robust optimization over multiple realizations showed practical gains.	Demonstrated on Brugge model with a limited set of realizations (five in the robust case); The study emphasized well placement/deliverability—chemistry/geomechanics was not addressed. Generality beyond the benchmark remains.
Han et al. (10)	H_2	Depleted natural gas reservoir	Robust optimization framework for UHS: couples compositional simulation with a CNN-LSTM-Attention surrogate + robust optimization to find controls that perform well under uncertainty	Complexity and data demand of the hybrid model; limited real-field validation; reaction/ heterogeneity coverage depends on training set
Kanaani et al. (13)	H_2+ CO_2	Depleted oil reservoir (UHS–CCS co-optimization)	Built ML proxy for UHS and co-optimized operations with NSGA-II for three objectives: NPV, H_2 recovery factor, and CO_2 storage—revealing economic vs. technical trade-offs and demonstrating accurate proxy-driven optimization.	Proxy/optimization outcomes are case-specific and depend on the chosen NPV model.

CCS = carbon capture and storage; CCN = convolutional neural network; EOR = enhanced oil recovery; LSTM = long short-term memory networks; ML = machine learning; NPV = net present value; NSGA-II = Non-dominated Sorting Genetic Algorithm II; UHS = underground hydrogen storage; WAG = water-alternating-gas injection.

surrogate modeling provides a powerful pathway toward real-time optimization, robust design, and techno-economic evaluation of hydrogen storage projects.

Moreover, several studies have utilized proxy models as an efficient tool for the optimization of carbon capture and storage (26, 28) and UHS (2, 7, 9, 10, 13, 22, 30) across different storage sites (see **Table 1**). For instance, Eltahan et al. (6) studied a set of realizations based on geological uncertainties and applied a stochastic gradient-based optimization method and full-reservoir simulations of underground hydrogen storage for the well-location optimization problem in a saline aquifer case.

While providing valuable insights and findings from optimization results, most of the above-cited studies lack a systematic approach. They also lack a validation step during the post-processing of the solutions. Therefore, the main objective and contribution of this paper is to present key findings from multi-objective optimization and address the limitations associated with physics-based compositional simulation in hydrogen storage optimization in a depleted gas reservoir. For this purpose, the potential of AI-based models was evaluated, and an artificial neural network algorithm was used to build a surrogate model, followed by the application of a multi-objective evolutionary optimization algorithm (i.e., Pareto-based) to determine the optimal operating conditions.

The rest of the paper is outlined as follows. Section 2 describes the simulation base case and how to collect the training and testing data for building the smart proxy models, which are briefly introduced in this section. The results and discussion of applying different proxy models are presented in Section 3. Finally, this research is concluded in Section 4.

2. SIMULATION AND OPTIMIZATION METHODOLOGY

2.1. Simulation model

This study investigates the capability and performance of data-driven proxy models for simulating UHS in a depleted gas reservoir with initial natural gas and water saturation values of 0.91 and 0.09, respectively. To achieve this, a compositional two-phase (hydrogen/water) fluid model was

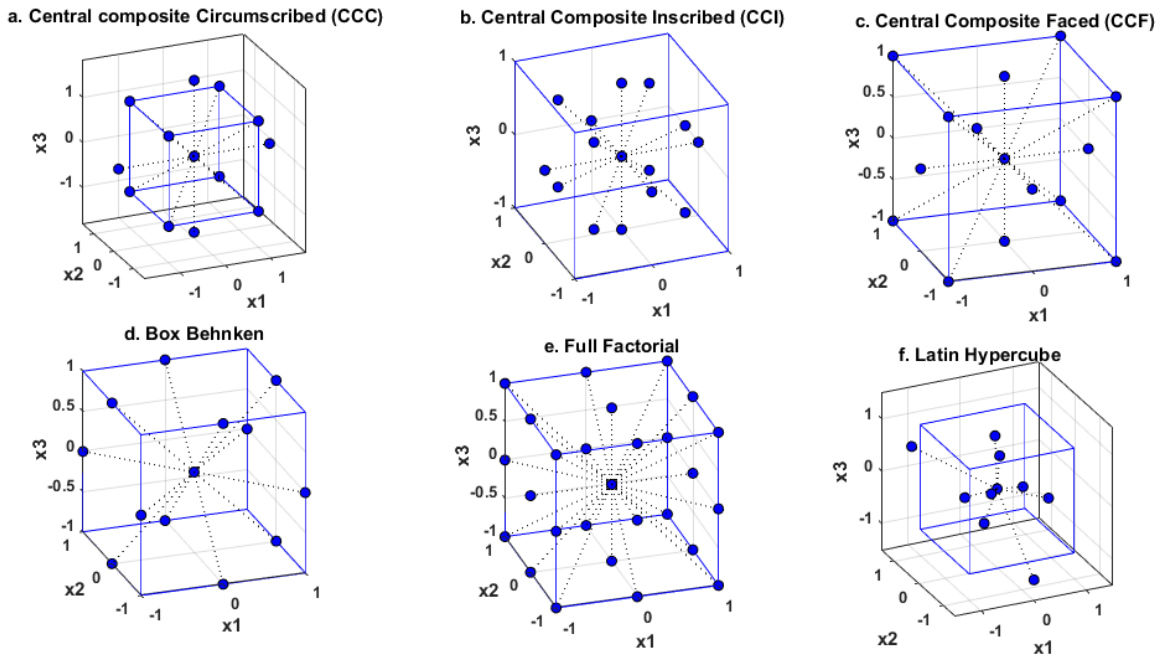

Figure 1: 3D schematics of different designs of experiment methods.

Table 2: Input data for base-case reservoir simulation model.

	Parameter	Value	Unit
1	Number of grid cells (N_r, N_θ, N_z)	(21, 20, 5)	-
2	Size of grid cells (Δr, $\Delta\theta$, Δz)	(40, 18°, 28)	ft
3	Reservoir Top Depth	4500	ft
4	Reservoir Porosity	0.20	-
5	Reservoir Permeability (k_x, k_y, k_z)	(200, 200, 20)	mD
6	Reservoir rock compressibility @ P=1000 psia	4.0×10^{-6}	1/psia
7	Initial Reservoir Pressure	1000	psia
8	Reservoir Temperature	210	°F
9	Initial gas and water saturation (S_g, S_{wc})	(0.91, 0.09)	-
10	Reservoir initial gas composition ($C_1, C_2, C_3, nC_4, nC_5, CO_2, N_2$)	(90, 2, 2, 2, 2,1, 1)	%
11	Henry's constant (CO_2, CH_4, N_2)	(2.94×10^4, 5.88×10^5, 1.47×10^6)	psia
12	Corey model parameters for relative permeability ($S_{wc}, S_{gc}, Kr_w^*, Kr_{H_2}^*, n_w, n_{H_2}$)	(0.2, 0, 0.50, 0.15, 1.5, 1.7)	-
13	Peng-Robinson equation of state parameters (Ω_a , Ω_b)	(0.4073, 0.08295)	-

setup based on the Peng–Robinson equation of state. Henry's law was utilized to define CO_2 solubility in water (16). The adaptive-implicit method (AIM) was employed to solve the linearized system of governing equations. A synthetic three-dimensional (3D) cylindrical homogeneous reservoir model (2100 grid cells) was developed in a computer modelling group-generalized equation-of-state model (CMG-GEM) as a base-case model to simulate the cyclic process for 14 years, including: **1)** cushion gas (CO_2, CH_4, or N_2) injection for 1 year to increase the initial reservoir pressure and retain the working gas production pressure, **2)** intermittent hydrogen gas injection and production for 10 years, and **3)** hydrogen gas production for 3 years, as described by Kanaani et al. (13).

Various operational parameters, including the completion interval, hydrogen gas injection and production flow rates, cushion gas composition, and cushion gas injection flow rate, were selected as decision variables. Subsequently, a proxy model was used to accelerate sensitivity analysis and optimization of the subsurface reservoir behavior based on the considered target parameters. Finally, an alternative statistical decision-making method was used to design and identify the best hydrogen injection/production scenario based on the overall utility parameter.

It is noteworthy that the primary goal of this study is to develop and validate surrogate models for a representative and physically consistent subset of UHS scenarios relevant to the specific storage concept and reservoir characteristics investigated. Therefore, the selected scenarios and the operational ranges were deliberately chosen to reflect realistic and practically relevant conditions reported in the literature and to align with the intended application of the models. The ranges of the parameters used in the design of experiments are listed in **Table 2**. Future work may extend the current framework by incorporating a broader range of reservoir types, operational strategies, and geological uncertainties to enhance model generality.

2.2. Input/output dataset preparation

Figure 1 shows the 3D schematics of different design-of-experiments (DOE) methods. In this study, the Latin hypercube method was applied to generate a table comprising 512 experiments based on defined variables across nine different scenarios, resulting in a total of 4,608 simulation jobs. The Latin hypercube DOE method was utilized to cover the full parameter space and randomly generate both integer and continuous values for the influential factors. The selected parameters include: **1)** cushion gas injection rate and composition, **2)** injection/withdrawal flow

Table 3: Overview of different UHS scenarios, including injection/withdrawal rates and schedules.

Scenario #: (Inj., Shut-in, Prod.)	Cushion gas Injection rate (MMscf/day)	Working gas injection rate (MMscf/day)	Production flowrate (MMscf/day)
S1: (4, 4, 4)	4.0	7.0	7.0
S2: (4, 0, 8)	4.0	7.0	3.5
S3: (5, 1, 6)	4.0	5.6	4.7
S4: (5, 2, 5)	4.0	5.6	5.6
S5: (5, 0, 7)	4.0	5.6	4.0
S6: (6, 0, 6)	4.0	4.7	4.7
S7: (6, 1, 5)	4.0	4.7	5.6
S8: (7, 0, 5)	4.0	4.0	5.6
S9: (8, 0, 4)	4.0	3.5	7.0

Inj. = injection, Prod. = production

rate of working gas, and **3)** well completion status (open/closed). These input parameters were randomly initialized based on sampling from normal and uniform distributions. Each run takes approximately ten minutes to generate the output results.

Equal pore volume injection is considered in order to eliminate the effect of storage volume and provide a uniform basis for comparison, thereby allowing the influence of other operational variables (such as the injection/production schedule, cushion gas composition, and well configuration) to be more clearly investigated. Input data were generated based on normal and uniform distributions for cushion and working gas injection flow rates. **Table 3** summarizes the injection/production rates and durations for different UHS scenarios, reflecting the complexity and variability of the storage process in a depleted gas reservoir.

Moreover, the Net Present Value (NPV) was employed for the economic evaluation of inflow and outflow values in hydrogen storage operations, calculated as the sum of the present values of all expected cash inflows and outflows over the project lifetime. **Equation 1** is used for calculating this criterion. It should be mentioned that the fixed capital expenditure term (compressor and well costs), equal to US$50MM (8) for all scenarios, was not considered in the optimization process of objective function, and the NPV function is defined by **Equation 1**:

$$NPV = \sum_{j=1}^{N} \sum_{t=1}^{T} \frac{Q_j \times U_j \times f_j}{(1+i)^t} \tag{1}$$

where t is the time of the cash flow, and Q, U, and f are the quantity of the objective function, the user specified unit value, and the conversion factor of each item. **Table 4** summarizes all cash inflow and outflow items considered in the NPV calculation.

 https://doi.org/10.69631/m0g16y60

2.3. Proxy Models

The majority of subsurface engineering problems (e.g., history matching, well placement, production optimization, and uncertainty analysis) are nonlinear, complex, and time-consuming to solve based on discrete calculus and numerical simulation. Both computational burden and the accuracy/quality of the obtained solutions depend on the grid cell size, i.e., the number of cells. Therefore, there is a trade-off between computational time and accuracy of the results. Using a coarse-grid model allows for faster computations at the expense of accuracy, as long as convergence is achieved. Moreover, many researchers seek efficient computational approaches that enable the execution of tens to hundreds of reservoir model realizations within a limited time frame, thereby facilitating frequent updates of field development plans, supporting near real-time decision-making, and reducing reliance on oversimplified engineering assumptions (5).

To address the aforementioned problem, proxy models (PMs), sometimes called meta-models or surrogate models, are proposed. These models are often described as fast table interpolation methods and are widely implemented for different applications. Several researchers have classified proxy models into four categories: **a)** multi-fidelity models, **b)** reduced-order models, **c)** traditional proxy models, and **d)** smart proxy models (5, 25).

In this study, due to the high total computational time of running compositional UHS models for different tasks, including compositional model setup, simulations, sensitivity analysis, uncertainty quantification, output data analysis, and multi-objective optimization, we employ the computational power of machine-learning-based proxy models for UHS operational-condition optimization in different injection/withdrawal scenarios. In the following subsections, the theory of the applied algorithms will be briefly explained.

2.3.1. Regression tree and ensemble learning methods

Tree-based models are one of the oldest and most powerful tools for classification and regression problems. A machine-learning tree is a nested structure of conditions and nodes for data partitioning and decision-making. Each node represents a split on a variable or attribute. The

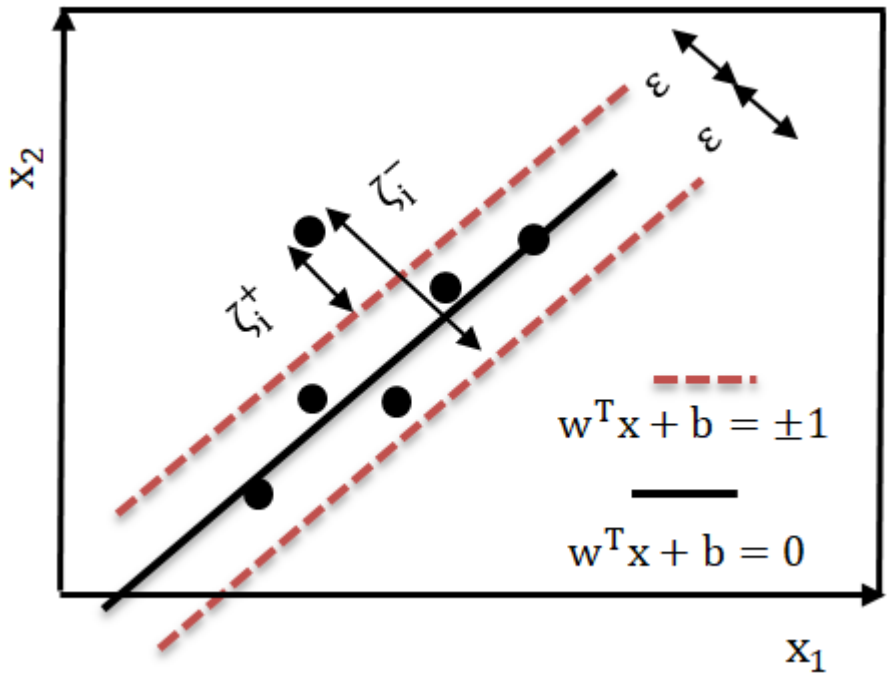

Figure 2: Support vector regression algorithm.

selection of the best variable for each node is based on minimizing the mean square error or sum of residuals of the training subset. Creating the tree starts from the root (beginning) node and proceeds downward to a leaf node (response) until one of the stopping rules is satisfied, after which a pruning process can be applied to the constructed tree (3, 14).

Illustrating knowledge in the simple form of a tree structure makes tree-based categorization reasonably interpretable and straightforward. However, their low accuracy and limited flexibility in forecasting limit their applicability. Hence, ensemble learning methods are used, which lead to better results. The Ensemble learning method involves a combination of weak base learners (e.g., decision trees) in parallel (bagging) or sequential (boosting) ensemble methods. In the bagging technique, several independent regression trees are grown by bootstrap sampling, i.e., random sampling with replacement and random selection of a subset of features. Finally, a voting or averaging method is performed to predict the response value (31).

2.3.2. Support vector regression

Originally, support vector machine regression represents a linear function to establish a relationship between input and output data by minimizing error function and risk of incorrect estimation. As can be seen in **Figure 2**, the main objective of this algorithm is to find a function that fits the data with a distance from the hyperplane $w^T x + b = 0$ or residual values less than the epsilon margin (ε). However, it is possible no such function exists to fit and satisfy the mentioned constraint for all data points (i.e., hard problem). Therefore, a slack variable, which is a positive value representing the violation (ζ_i) is considered for each observation. By including this term in the main objective function, the error function is allowed to exist, thereby providing the flexibility required to obtain feasible solutions. **Equation 2** represents the primal form, and the positive constant value of C is considered as a penalty parameter (27).

$$min\frac{1}{2}w^T w + C\sum_{i=1}^{N}(\zeta_i^+ + \zeta_i^-) \qquad s.t. = \begin{Bmatrix} \forall_i: -\varepsilon - \zeta_i^- \le t_i - y_i \le \varepsilon + \zeta_i^+ \\ \forall_i: \quad \zeta_i^+ \ge 0 \\ \forall_i: \quad \zeta_i^- \ge 0 \end{Bmatrix} \tag{2}$$

where t_i, y_i, ζ_i^+, and ζ_i^- are the target values, predicted values, and slack variables for each observation. N is the number of observations, w is the vector of weights, C is a positive value referred to as the box constraint, and ε is half of the allowed deviation.

The primal form of the objective function can be turned into a dual formula by using the Lagrangian technique to add constrained expressions with non-negative multipliers in primal form. In addition, by applying a partial derivative to variables we will have **Equation 3** and **Equation 4**:

$$L_P = \min\ \frac{1}{2}w^T w + C\sum_{i=1}^{N}(\zeta_i^+ + \zeta_i^-) - \sum_{i=1}^{N}\alpha_i^+(-t_i + y_i + \varepsilon + \zeta_i^+) - \sum_{i=1}^{N}\alpha_i^-(t_i - y_i + \varepsilon + \zeta_i^-) - \sum_{i=1}^{N}\mu_i^+\zeta_i^+ - \sum_{i=1}^{N}\mu_i^-\zeta_i^- \tag{3}$$

$$L_D(\alpha) = min\sum_{i=1}^{N}\sum_{j=1}^{N} -\frac{1}{2}(\alpha_i^+ - \alpha_i^-)\left(\alpha_j^+ - \alpha_j^-\right)X_i^T X_j + \sum_{i=1}^{N}(\alpha_i^+ - \alpha_i^-)t_i - \varepsilon\sum_{i=1}^{N}(\alpha_i^+ - \alpha_i^-) \qquad s.t = \begin{Bmatrix} \forall_i: \sum_{i=1}^{N}(\alpha_i^+ - \alpha_i^-) = 0 \\ \forall_i: \ 0 \le \alpha_i^- \le C \\ \forall_i: \ 0 \le \alpha_i^+ \le C \end{Bmatrix} \tag{4}$$

In this equation, X is the input matrix, and α_j^+, α_j^- are the variables. By substituting a nonlinear kernel function, such as a Gaussian or polynomial kernel, instead of $X_i^T X_j$, a nonlinear regression vector machine can be implemented.

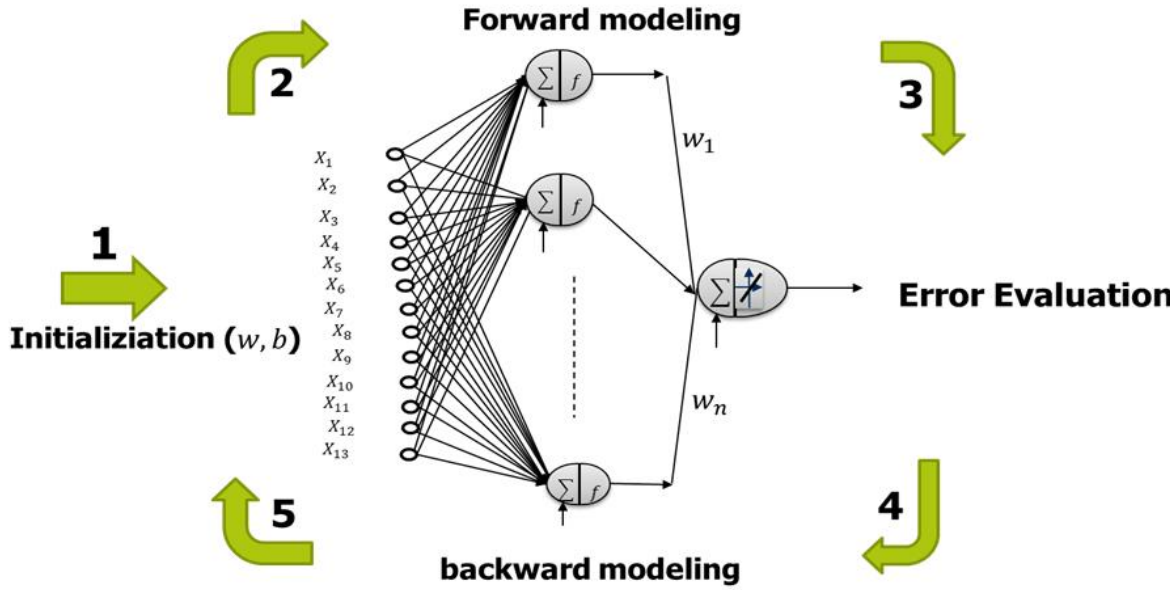

Figure 3: Schematic diagram of neural network model training.

2.3.3. *Artificial neural network (ANN)*

To overcome the associated problems of numerical modeling, smart proxy models (e.g. artificial neural network) are suggested as tools for the successful replication of underground geological hydrogen storage simulation models. Accordingly, the targeted neural network model to predict the hydrogen recovery factor, hydrogen purity, and the net present value (NPV) is created by determining the network architecture (feed-forward or cascade-forward), the number of neurons in the hidden layers, and the type of transfer function (e.g., tangent sigmoid). Next, the weights of the network are calculated and updated according to the following steps, using the gradient descent method (1):

1. Specify the network architecture and hyperparameters, including the number of neurons and the activation functions of each layer.
2. The weights and bias values of the neural network are randomly initialized (**Fig. 3**).
3. Forward modeling, i.e., the inputs to the activation functions are computed, and then the output values are calculated for each neuron in each layer (**Eq. 5** and **Eq. 6**).
4. Backward modeling, i.e., the error value for the output layer is determined by comparing the target (measured) and output (predicted) values (**Eq. 7**).
5. The gradients of the network parameters and weights are calculated for the hidden layers (**Eq. 8** and **Eq. 9**).
6. Using the calculated gradients and the learning rate, the biases and weights of the network are calculated and updated (**Eq. 10**).
7. Steps 3 through 6 are repeated until one of the specified stopping criteria for network training is satisfied.

$$Z^{(l)} = W^{[l]} A^{[l-1]} + b^{[l]} \quad (5)$$

$$A^{(l)} = g^l(Z^{[l]}) \quad (6)$$

$$dZ^{(l)} = dA^{(l)} * g^{l'}(Z^{(l)}) \quad (7)$$

$$dA^{(L)} = A^{(L)} - Y \qquad dA^{(l-1)} = W^{[l]^T} * dZ^{(l)} \quad (8)$$

$$dW^{(l)} = dZ^{(l)} * A^{[l-1]^T} \qquad db^{[l]} = dZ^{(l)} \tag{9}$$

$$W^{(l)} = W^{(l)} - \alpha * dW^{[l]} \qquad b^{(l)} = b^{(l)} - \alpha * db^{(l)} \tag{10}$$

In the above equations, the superscript l denotes the number of hidden layers, L represents the output layer, and $W^{[l]}$, $b^{[l]}$, $Z^{[l]}$ and $A^{[l]}$ are the weights, bias values, activation-function inputs, and activation-function outputs, respectively. All these parameters are employed in the middle layer of the targeted neural network model. Furthermore, the parameters $dZ^{[l]}$, $dA^{[l]}$, $dW^{[l]}$ and $db^{[l]}$ denote the corresponding gradient values. In addition, the parameter of α is related to the learning rate of the network and the symbols g^l and $g^{l'}$ represent the applied activation function and the first derivative of the activation function in each layer, respectively.

Figure S1 in the **Supplementary Material** (available online) illustrates the flowchart of the implemented procedure for the multi-objective optimization of UHS. In this regard, a DOE-based set of multiphase compositional flow simulations with the Computer Modelling Group – Generalized Equation-of-State Model (CMG-GEM), as outlined previously, was performed. Then, the collected data are utilized to train data-driven models as alternatives to physics-based models. Finally, the best-performing predictor model, coupled with the Non-dominated Sorting Genetic Algorithm II (NSGA-II) optimization algorithm, is repeatedly applied for the co-optimization of hydrogen purity, hydrogen recovery factor, and NPV.

3. RESULTS AND DISCUSSION

3.1. Hydrogen recovery factor

As mentioned earlier, we considered a storage system that undergoes three phases: **a)** cushion gas injection, i.e., pressure maintenance in a depleted gas reservoir (12 months), **b)** injection/withdrawal cycles of working gas (under different scenarios), and **c)** long-term production (36 months). **Figure 4** shows the hydrogen recovery factor versus time for the base-case model (represented by the black line), and for different operational conditions as outlined in **Table 3**. In general, the hydrogen recovery factor versus time shows an increasing trend and then diminishes or plateaus due to operational constraints. At the early stages of the storage cycle, the hydrogen recovery factor shows a steady increase with time. This behavior can be attributed to the high initial reservoir pressure, efficient displacement of cushion gas, and limited interaction between the injected hydrogen and the residual gas phases. Under such conditions, the production stream remains relatively pure, and the recovery response is strongly governed by favorable pressure gradients and continuous injection–production operations.

As the operation continues, the recovery trend often exhibits fluctuations (ups and downs), and a reduced growth rate. These variations are commonly attributed to operational strategies such as cyclic injection and withdrawal, as well as reservoir-scale effects, including visco-capillary fingering, mechanical dispersion and partial mixing between hydrogen and cushion gas. Periodic changes in the operational parameters (e.g., production rates, shut-in periods, or pressure management constraints) may also lead to temporary rises or falls in the recovery factor, which are reflected as fluctuations in the curve.

Towards the later stages, the recovery factor generally continues to increase before eventually plateauing, reflecting the impact of operational and reservoir limitations. This behavior can be explained by reduced gas mixing, and increased production of cushion gases (such as CH_4, CO_2, or N_2) – explained further below.

For a few simulation cases, the recovery factor approaches 1.0; however, this does not indicate that operational or physical constraints were inactive. Rather, it is primarily a result of a long production (withdrawal) period and the absence of capillary trapping.

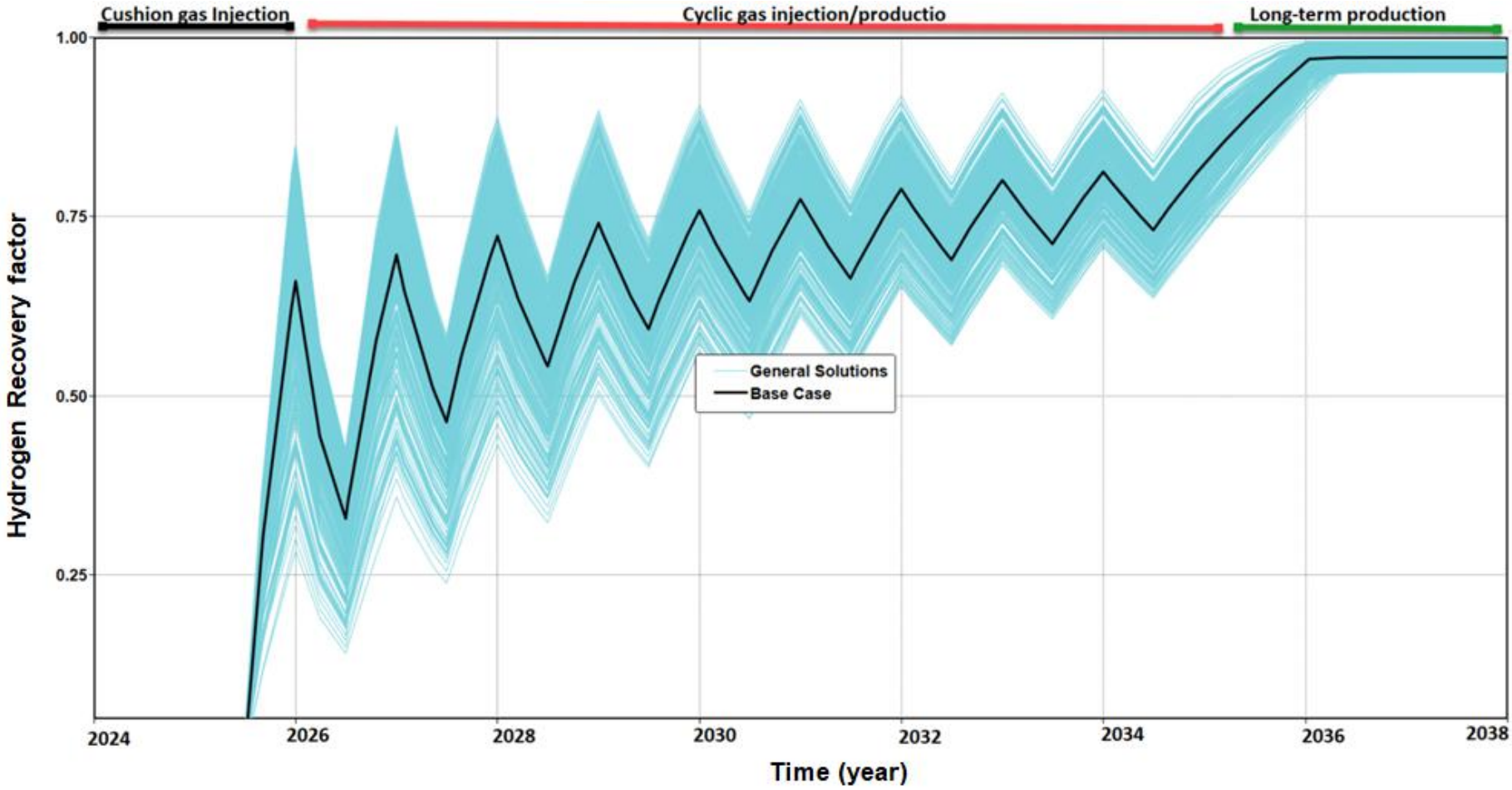

Figure 4: Hydrogen recovery factor during cyclic injection and production, and long-term production.

https://doi.org/10.69631/m0g16y60

As discussed in Section 2.1, the reservoir was conceptualized as a cylindrical model comprising a vertical wellbore surrounded by a porous medium with radial flow geometry (see **Fig. 5**). This simplification reflects the dominant pressure and flow distribution patterns expected in a typical storage reservoir, where injection and withdrawal operations are controlled primarily by radial gradients around the well. The cylindrical model enables a more realistic representation of hydrogen displacement and mixing with cushion gases compared to a purely Cartesian framework due to grid-orientation effects.

The distribution of hydrogen within the cylindrical domain is strongly influenced by both radial pressure gradients and gravitational segregation. Immediately after injection, hydrogen tends to occupy the upper parts of the reservoir due to its extremely low density and molecular weight, while heavier cushion gases such as CH_4, N_2, and CO_2 remain preferentially in the lower zones. Radially, the hydrogen concentration is highest near the wellbore and gradually decreases with distance as dispersion, diffusion, and mixing with cushion gases increase.

Moreover, maintaining high hydrogen purity (represented by the mole fraction of hydrogen in the produced gas) during underground storage is critical. The presence of cushion gases in the outflow is referred to as impurities or contaminants for UHS operation. Gas purity is affected by in-situ mixing of hydrogen with the resident gases due to molecular and mechanical dispersion. These aspects are mimicked in the model by the numerical dispersion, D_{num}which is sensitive to the grid block size (Δx), time step size (Δt), velocity (u), and the Courant number (N_{co}) (**Eq. 11**):

$$D_{num} = \frac{u\Delta x}{2}[1 - N_{co}] \qquad N_{co} = \frac{u\Delta t}{\Delta x} \tag{11}$$

Numerical dispersion increases with coarser grids and decreases as the Courant number approaches unity. Thus, accurate front tracking requires adjusting the grid size, time step, and the Courant number (23). If the actual mixing parameters in a given field are known, the physical dispersion parameters can be set. In absence of such data, we modelled mixing using numerical dispersion.

As seen in **Figure 6**, the purity of hydrogen undergoes noticeable variations during different operational phases. In the first injection–production cycle, the hydrogen purity is initially very high because the production stream mainly consists of newly injected hydrogen, with negligible interaction with cushion gases. However, as soon as production starts, a sudden decline in purity is observed. This rapid drop is attributed to the early breakthrough of residual cushion gas (that had occupied pore spaces and flow pathways prior to hydrogen injection.

During the subsequent cycles, the general behavior of hydrogen purity becomes more stable, showing gradual increases during the withdrawal periods and slight decreases during injection. This oscillatory pattern is explained by the dynamic displacement and mixing processes: during withdrawal, hydrogen dominates the production stream, and purity improves, while during injection, the displacement front pushes some cushion gas toward the production well, reducing purity temporarily.

Finally, after all simulations were completed for the scenarios considered, a clean dataset including 4253 datapoints was prepared to build the proxy models. **Figure S2** in the **Supplementary Material** (available online) shows the histogram plots and deviations from the fitted Gaussian distributions of the target variables (hydrogen recovery factor, hydrogen purity, and NPV) for the original dataset.

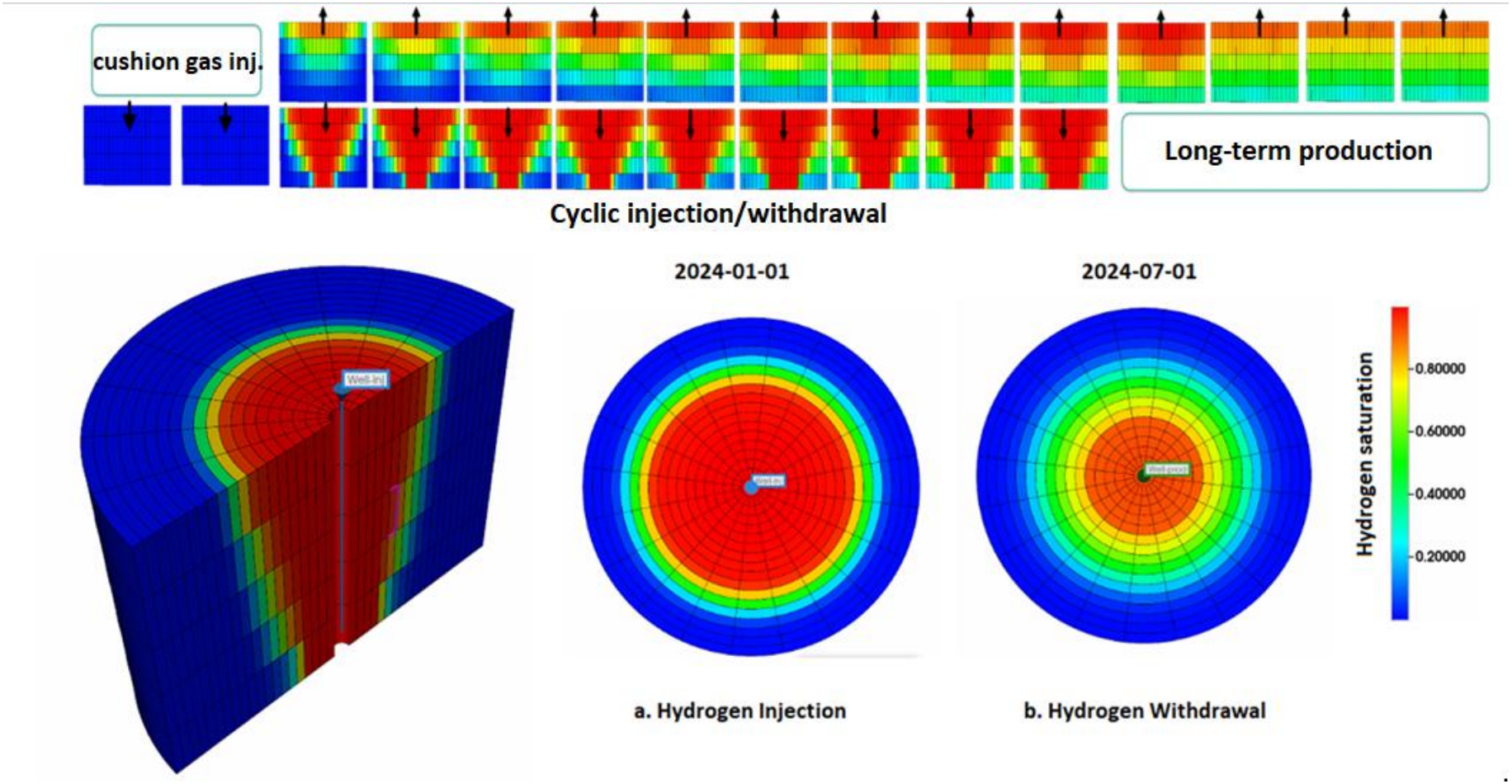

Figure 5: Snapshots from the hydrogen injection–withdrawal life cycle.

https://doi.org/10.69631/m0g16y60

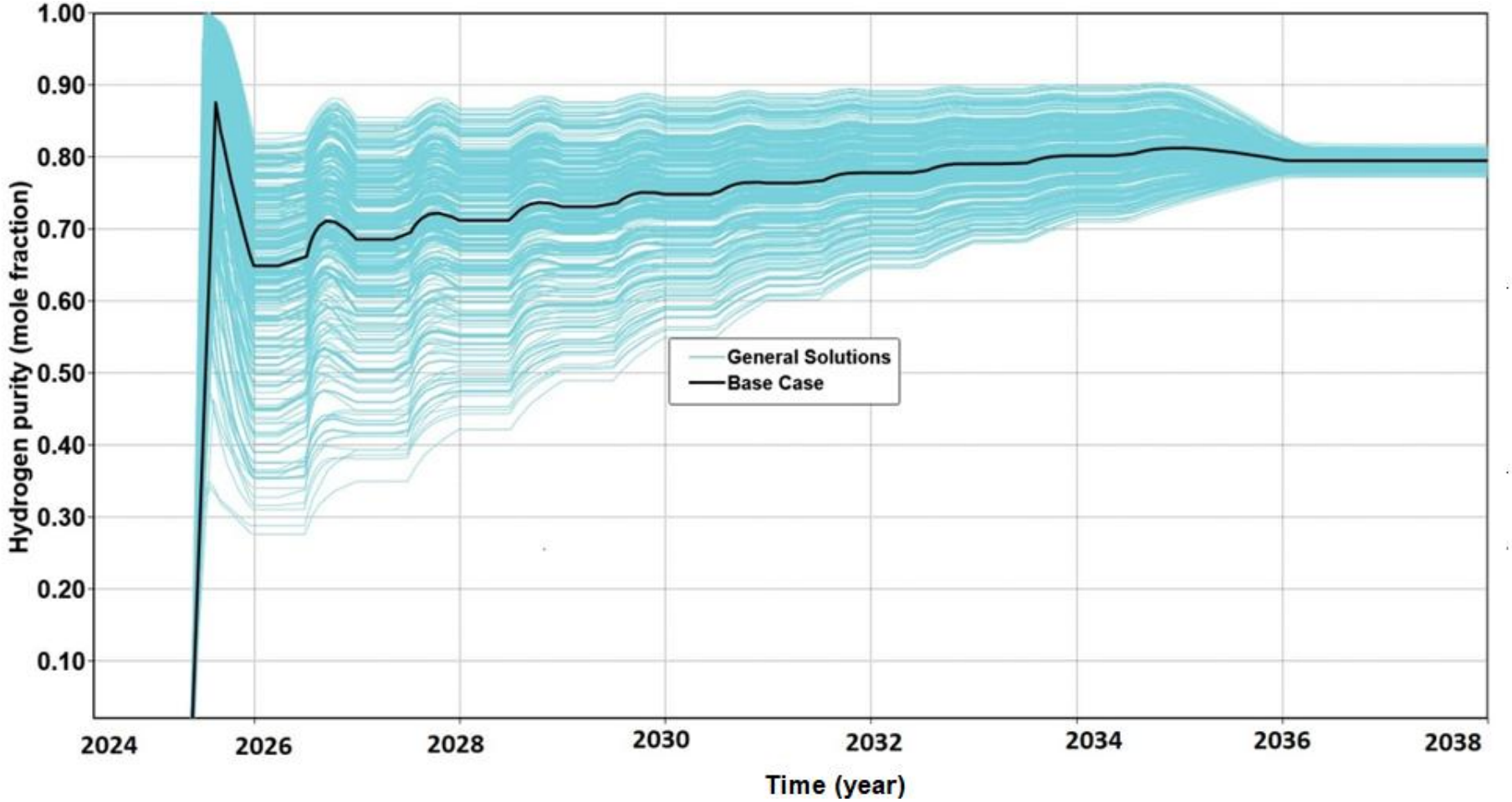

Figure 6: Hydrogen purity during cyclic injection/production and long-term production.

https://doi.org/10.69631/m0g16y60

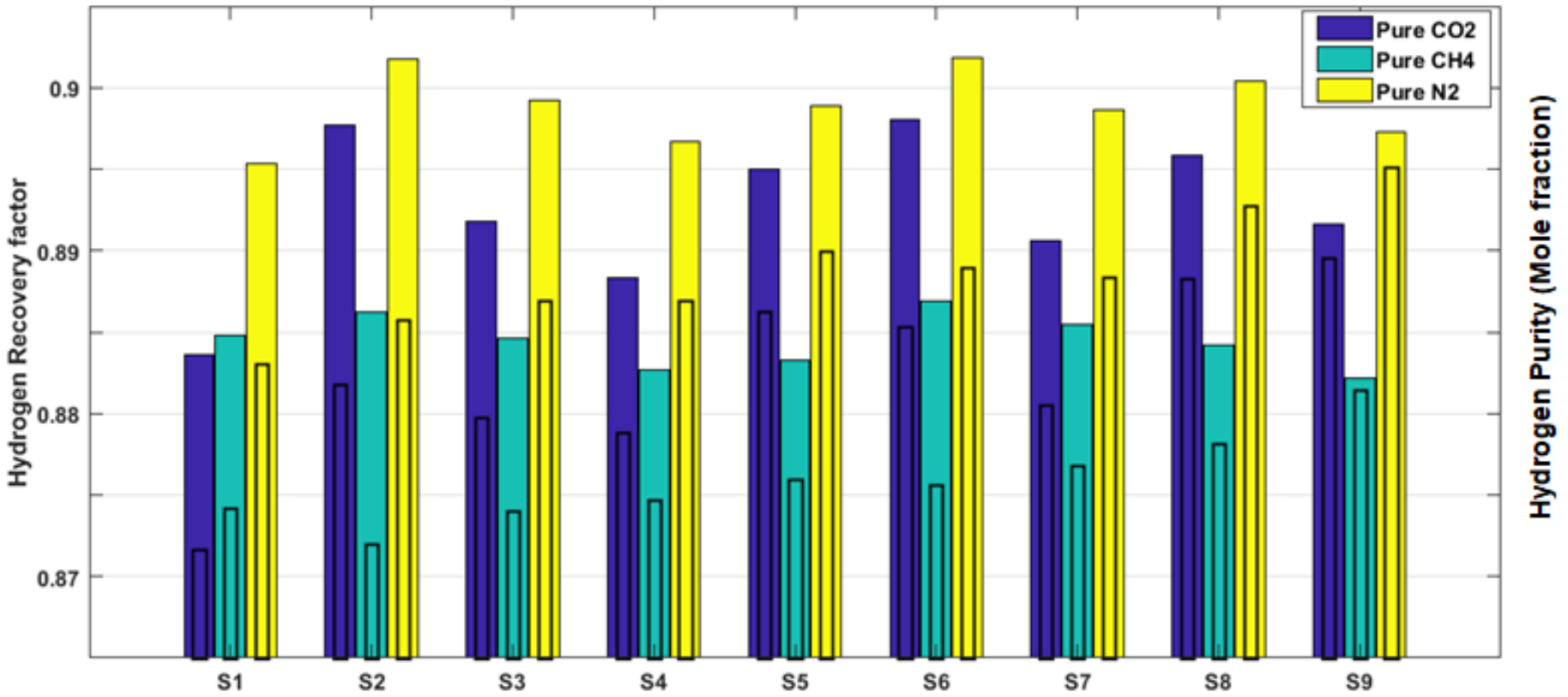

Figure 7: Effect of pure cushion gas injection on hydrogen recovery factor and hydrogen purity for all simulation scenarios.

https://doi.org/10.69631/m0g16y60

3.2. Effect of cushion gas composition on UHS efficiency

Figure 7 compares the simulation results when a pure cushion gas is used in the early stage of UHS. As shown in the figure, pure N_2 (yellow bar), CO_2 (blue bar) and CH_4 (green bar) provide the best-to-worst candidate scores as cushion gases in a depleted reservoir based on the hydrogen recovery factor (the first bar) and hydrogen purity (the overlayed bar). During the withdrawal step, the gas segregation mechanism becomes a dominant factor influencing the purity of the produced hydrogen. This phenomenon is primarily controlled by differences in density and molecular weight between hydrogen and the selected cushion gas. Since hydrogen has the lowest molecular weight (2 g/mol) and very low density compared to other gases (e.g., N_2 = 28 g/mol, CH_4 = 16 g/mol, CO_2 = 44 g/mol), gravitational segregation tends to stratify the gases within the reservoir. Hydrogen accumulates preferentially in the upper zones of the porous medium, while heavier cushion gases tend to settle in the lower regions. Moreover, differences in compressibility and non-ideality behavior (CO_2> CH_4> N_2) of cushion gas components lead to gas spreading, and thus variations in hydrogen purity and recovery factors (20). Hence, the design of an optimum cushion gas composition will be further investigated in this research.

3.3. Sensitivity Analysis Results

At first, the hydrogen storage efficiency was described based on the hydrogen recovery factor and hydrogen purity, i.e., the target variables. Then, the controllable influential variables were identified. **Figure 8** represents the tornado plots of a linear proxy model, which demonstrate the relative importance of the operational parameters of geological hydrogen storage for hydrogen purity and hydrogen recovery factor. As can be seen, hydrogen production flowrate (0.0269) and nitrogen composition (0.0390) have relatively significant influence indicators on hydrogen recovery factor and hydrogen purity, respectively. This implies that increasing or decreasing the hydrogen flow rate, i.e. the driving viscose force for hydrogen withdrawal leads to a significant change in the hydrogen recovery factor.

Afterwards, the Latin hypercube design–of–experiment (DOE) method was utilized to generate a table including the queued physic-based simulations that were required to be run sequentially. This procedure was repeated for all scenarios to prepare a data bank. As presented in **Table 5**, the top two solutions from the DOE implementation are reported based on the simulated hydrogen recovery factor and hydrogen purity for each scenario.

For more detailed comparison, **Figure 9** represents the hydrogen purity (the bottom plot) and hydrogen recovery factor (the top plot) during the life cycle of UHS in a depleted gas reservoir. Scenario #5 (5–month injection + 7–month production) and scenario #7 (7–month injection + 5–month production) provide high hydrogen recovery factor and high hydrogen purity, respectively. In addition, scenario #1 (4 mon. injection + 4 mon. shut-in + 4 mon. production) is associated with a low recovery factor and low purity compared with the other scenarios.

Scenario #7 spreads the same volume over a longer injection interval (i.e., with a lower average injection rate). Lower injection rates reduce viscous fingering and help vertical segregation to develop; hydrogen, being much lighter, preferentially occupies the upper layers while heavier cushion gases settle in the lower layers. The longer, gentler injection therefore favors stratification and limits early radial mixing. During the subsequent (shorter) 5-month production period, the hydrogen trapped in the upper zones is produced with fewer contaminants, which explains the higher hydrogen purity observed for this scenario, despite a lower net recovery compared with scenario #5.

Scenario #1 performs the worst under equal-volume conditions because the shut-in interval promotes diffusive and dispersive mixing between hydrogen and cushion gas before production starts.

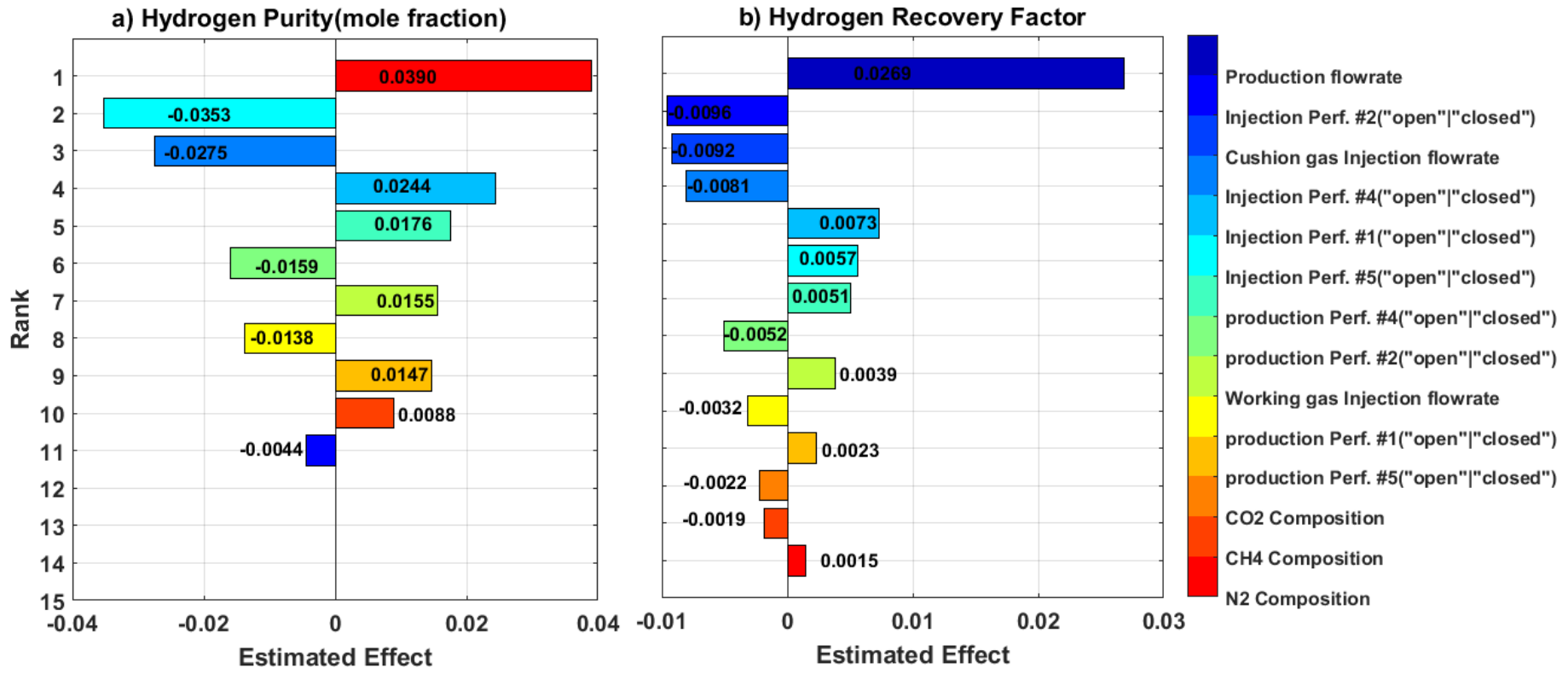

Figure 8: Sensitivity analysis results for different operational parameters.

https://doi.org/10.69631/m0g16y60

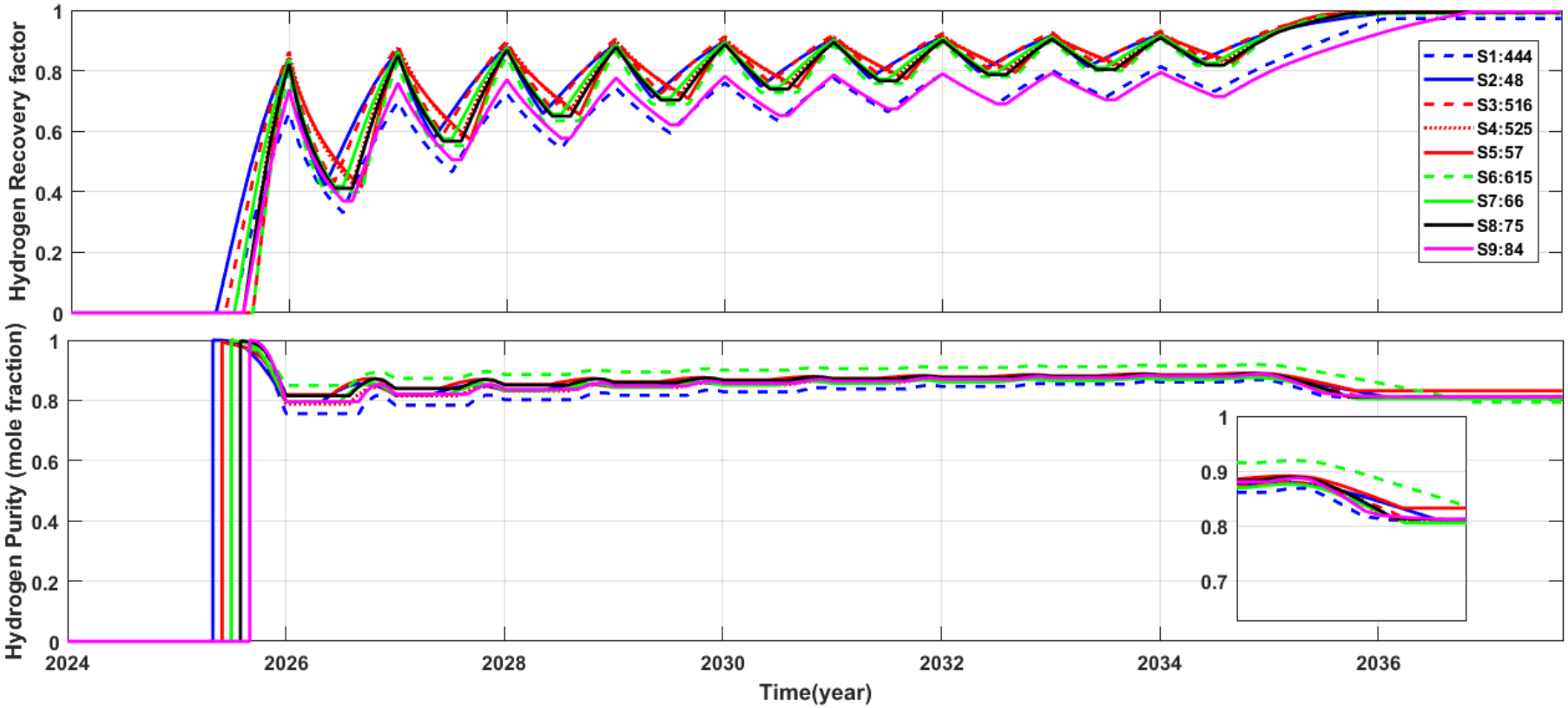

Figure 9: Hydrogen purity and recovery factor vs. time for design-of-experiment proposed simulations.

https://doi.org/10.69631/m0g16y60

Table 5: Physics-based simulation results for hydrogen storage based on the Latin hypercube design of experiment.

	Production well perforation status	Injection well perforation status	Cushion gas composition (CH_4, CO_2, N_2)	Cushion gas injection flowrate (MMscf/day)	Working gas injection flowrate (MMscf/day)	Production flowrate (MMscf/day)	H_2 Recovery factor (-)	H_2 Purity (mole fraction)
S1	■■■■■	■■■■■	(0.26, 0.28, 0.46)	3.94	6.89	7.17	0.9077	0.8612
	■■■■■	■■■■■	(0.16, 0.74,0.10)	3.94	7.18	7.07	0.8827	0.8838
S2	■■■■■	■■■■■	(0.33, 0.29, 0.38)	4.10	6.89	3.57	0.9204	0.8729
	■■■■■	■■■■■	(0.00, 0.74, 0.26)	3.90	7.14	3.41	0.8743	0.8981
S3	■■■■■	■■■■■	(0.35, 0.65, 0.00)	3.90	5.52	4.76	0.9169	0.8734
	■■■■■	■■■■■	(0.43, 0.57, 0.00)	3.92	5.74	4.72	0.8895	0.8903
S4	■■■■■	■■■■■	(0.07, 0.72, 0.21)	4.08	5.49	5.66	0.9095	0.8729
	■■■■■	■■■■■	(0.40, 0.27, 0.33)	4.10	5.66	5.54	0.8091	0.8911
S5	■■■■■	■■■■■	(0.16, 0.43, 0.41)	3.20	5.52	4.10	0.9295	0.8845
	■■■■■	■■■■■	(0.00, 0.41, 0.59)	3.00	5.57	3.92	0.8916	0.9013
S6	■■■■■	■■■■■	(0.18, 0.64, 0.18)	4.02	4.55	4.79	0.9276	0.8697
	■■■■■	■■■■■	(0.36, 0.31, 0.32)	4.04	4.69	4.55	0.8111	0.8987
S7	■■■■■	■■■■■	(0.00, 0.81, 0.19)	4.08	4.55	4.68	0.9163	0.8703
	■■■■■	■■■■■	(0.20, 0.41, 0.39)	4.0	4.67	5.52	0.8911	0.8942
S8	■■■■■	■■■■■	(0.28, 0.41, 0.31)	3.94	3.94	5.71	0.9206	0.8815
	■■■■■	■■■■■	(0.41, 0.17, 0.41)	3.90	4.10	5.52	0.8742	0.9018
S9	■■■■■	■■■■■	(0.28, 0.47, 0.25)	3.92	3.45	7.18	0.9168	0.8787
	■■■■■	■■■■■	(0.13, 0.86, 0.00)	4.06	3.59	6.83	0.8633	0.9052

Black ■ = closed; **green** ■ = open

https://doi.org/10.69631/m0g16y60

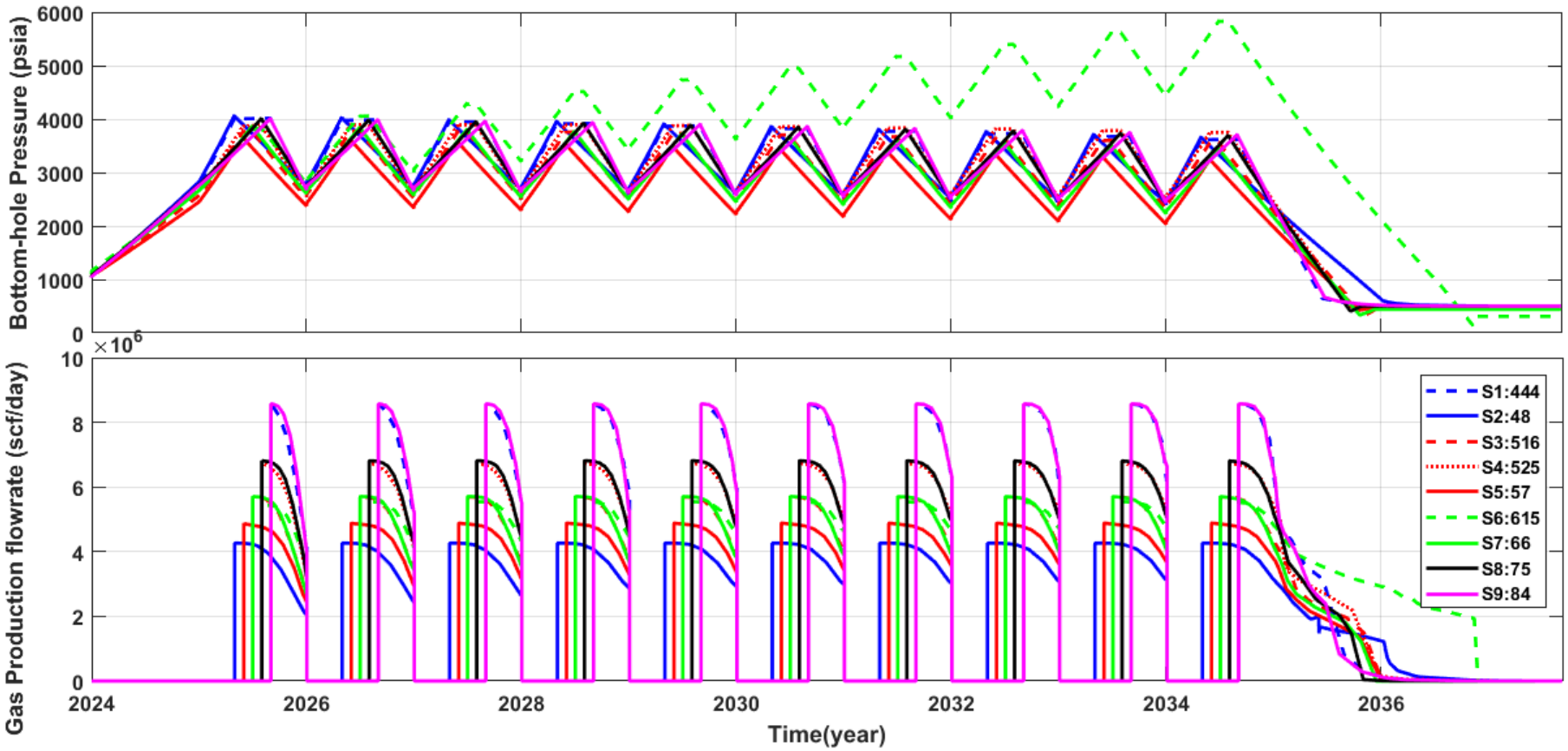

Figure 10: Hydrogen Injection bottom-hole pressure and production flow rate during different operational periods.

https://doi.org/10.69631/m0g16y60

Figure 10 (the top plot) represents the bottom-hole pressure during injection and production cycles. At early times, pure or mixed cushion gases are injected for initial pressurization (1000 to 4000 psia), and pressure support during the following cycles. The pressure build-ups and drawdowns are repeated, and the pressure drop in the last cycle is about 200 psia due to the cushion gas production in previous cycles. Finally, during the long-term production period, the bottom-hole pressure starts to decrease until the specified operational constraint (500 psia) is reached.

As shown in **Figure 10** (the bottom plot), the hydrogen flowrate behavior depends on the pressure drop at the production well. Initially the hydrogen production flowrate exhibits a short plateau period and then begins to decline rapidly, following the pressure decline of the storage reservoir.

To find the best scenario, and optimal operational conditions of UHS in a depleted reservoir, several tree-based methods (e.g., regression trees and ensemble methods), support vector regression, and Gaussian-based machine learning algorithms were applied. **Figure S3** in the **Supplementary Material** (available online) shows a subset (50 datapoints) from the simulation results of hydrogen recovery factor and hydrogen purity (black line), as well as boxplots, i.e., the deviation intervals of the predicted values of hydrogen purity and hydrogen recovery factor using different machine learning algorithms.

To fine-tune the ensemble tree-based methods, a grid search optimization algorithm was employed to find the optimal hyperparameters for the selected ranges, including the learning rate (0.1, 0.25, 0.5, 1.0), the number of trees in the ensemble (1 to 100) and the maximum number of splits ($2^0, 2^1, \ldots, 2^6$). As can be seen in **Figure 11**, the cross-validation mean squared error (MSE) curves decrease with an increasing number of weak tree learners until they reach the optimal number of trees. The grid search results indicate the optimal bagged tree model (MSE = 8×10^{-5}) with optimal parameters, including the number of trees, learning rate, and maximum number of splits equal to 149, 0.25 and 4 respectively.

In addition, multiple architectures of ANN models were trained, and network hyperparameters were tuned (using 10 neurons and a tangent sigmoid transfer function in the hidden layer) to improve model accuracy. Bayesian regularization optimization (with the Marquardt adjustment parameter set to 0.005) was employed for training the feed-forward ANN model. **Figure 12** shows the performance of the constructed feed-forward network model based on cross-plots of hydrogen recovery factor, hydrogen purity, and NPV for the training subset (R-values = 0.9413, 0.9889, and 0.9996), test/verification subset (R-values = 0.9465, 0.9868, and 0.9995), and the entire original dataset (R-value = 0.9420, 0.9887, and 0.9996), respectively.

It is noteworthy that some simulations yield undesired solutions with negative NPVs. This can occur under conditions where the recoverable hydrogen volume is low, hydrogen purity decreases due to excessive mixing with cushion gases, or when high operational costs (e.g., compression and separation) are not offset by sufficient revenue from hydrogen sales. These outcomes highlight the importance of optimizing cushion gas composition, injection–production strategies, and well configuration to ensure that technical feasibility is aligned with economic viability.

Hence, the obtained results from blind validation, i.e., the test subsets, confirmed the ability of the ANN model to act as a proxy model to predict the target variables and provide reliable estimations (without overfitting or underfitting issues) for the given decision variables in the optimization process.

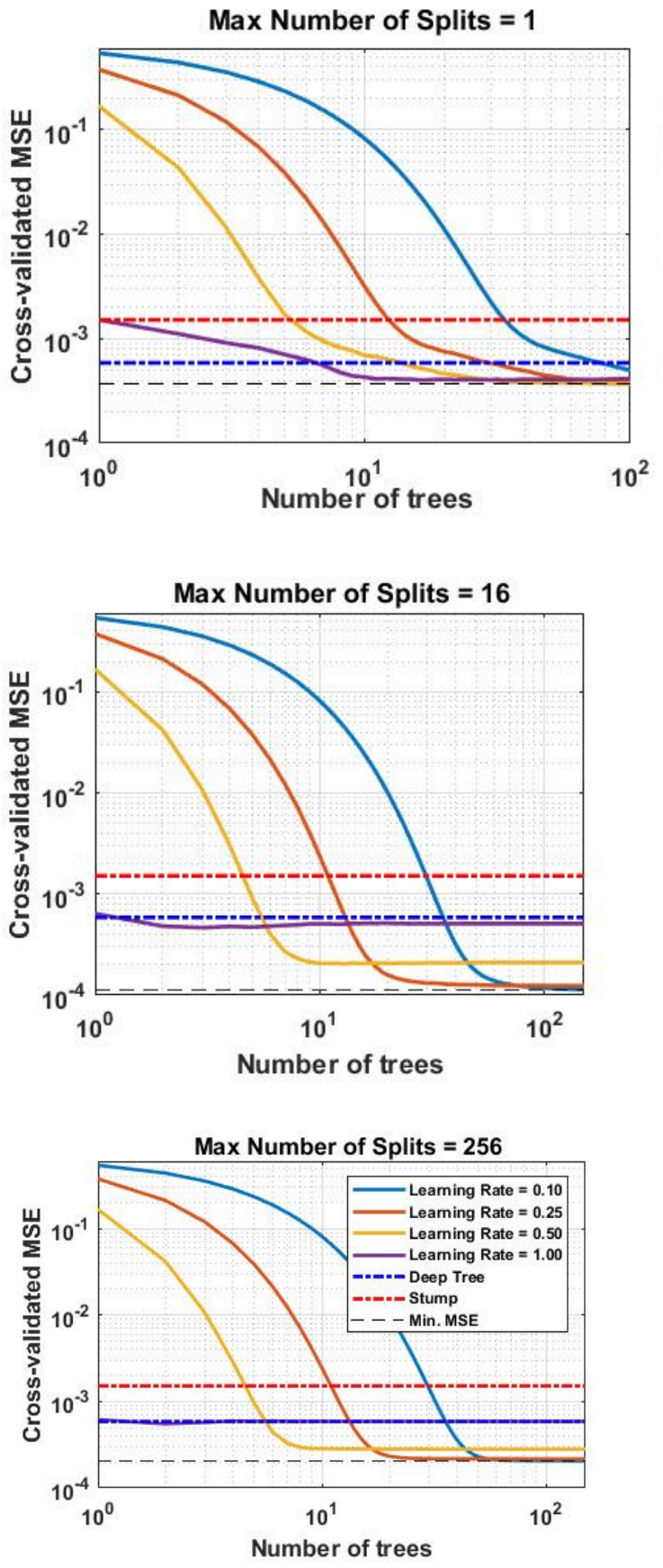

Figure 11: Grid search optimization results for ensemble learning algorithms.

 https://doi.org/10.69631/m0g16y60

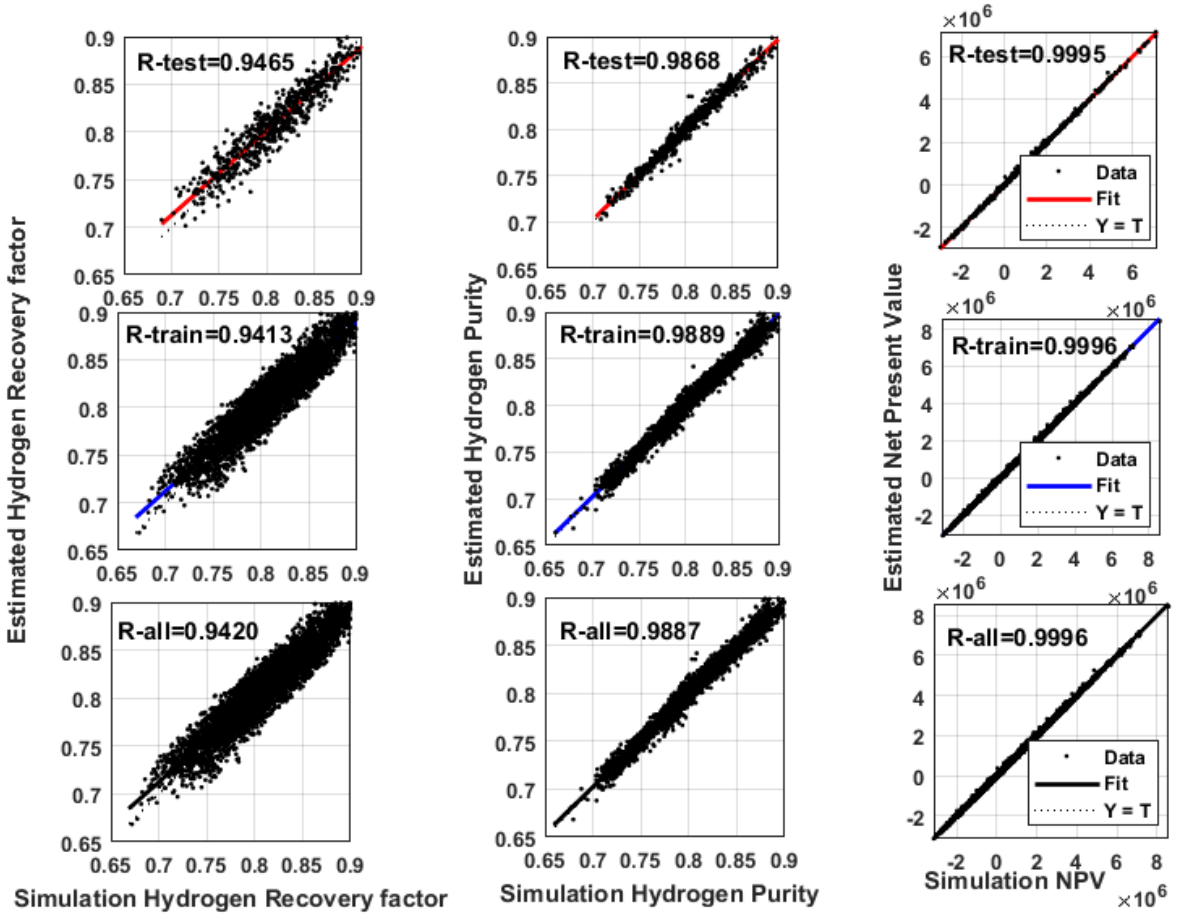

Figure 12: Cross-plots illustrating the hydrogen recovery factor, hydrogen purity, and net present value.

A schematic diagram of the trained network model and its parameters (bias and weight values) is provided in **Figure S4** in the **Supplementary Material** (available online). As additional information, **Figure S5** (available online) illustrates the training–testing loss (and accuracy) curves over successive epochs, where both curves exhibit a consistent and convergent trend without significant divergence. The absence of a widening gap between training and testing errors indicates that the model does not merely memorize the training data but instead captures the underlying relationships governing system behavior. Moreover, the stabilization of testing performance at later epochs suggests that the selected network architecture and training strategy provide an appropriate balance between model complexity and generalization capability, confirming that overfitting is effectively mitigated.

The ANN model serves as a fast alternative predictor of the target variables on a second-scale timespan, with computation time depending on the configuration of the computer system, including processor speed, memory, and hardware capabilities. As mentioned earlier, a multi-objective problem (hydrogen purity, hydrogen recovery factor, and NPV) must be formulated to find the best solution(s) using a multi-objective derivative free optimization algorithm. The NSGA-II algorithm is initialized randomly and generates the main population (200 solutions) and then selects parent solutions for crossover and mutation, where the crossover and mutation populations correspond to 0.80 and 0.05 times the population size, respectively. A new population is created by merging and truncating the resulting populations. The genetic algorithm (GA) repeatedly modifies the solutions from each previous generation to create subsequent

generations and ranks them into multiple fronts based on the number of dominated and dominating solutions.

For the final selection among operational scenarios, NPV is adopted as the primary decision metric because it provides a single, economically meaningful objective that directly reflects the commercial viability of each scenario. Secondary technical metrics, such as hydrogen recovery factor and hydrogen purity, are considered as tie-breaking criteria: they are used only when multiple scenarios exhibit similar NPVs. This hierarchical approach ensures that the selected scenario maximizes economic value while maintaining operational quality and product specifications.

As can be seen in the two-dimensional plot in **Figure 13**, a set of non-inferior solutions (green points) is presented as optimal solutions for UHS operational conditions based on hydrogen purity and recovery factor. These points are also called the Pareto front, representing the first-ranked solutions among the other feasible solutions (black dots).

Figure 14 represents the optimum solutions corresponding to target values in a two-objective optimization of UHS. As can be seen, the suggested compositions are approximately equal to 45%, 40% and 15% for N_2, CH_4 and CO_2, respectively. The hydrogen recovery factor and purity criteria vary between 0.8 to near 1.0. When NPV is incorporated into the optimization algorithm, representing the solution of a three-objective optimization of the UHS process, the results show that a CO_2 fraction close to 100% can be the best solution, considering both economic criteria and the added value CO_2 through carbon capture and storage (see **Fig. 15**). Increasing the fraction of CH_4 and N_2 in the cushion gas causes a decrease in the NPV because it reduces both recoverable hydrogen and the overall operational efficiency. Cushion gas is necessary to maintain reservoir pressure and ensure stable injection and production cycles; however, higher fractions of CH_4 and N_2 occupy pore space that could otherwise be filled with hydrogen, thereby lowering the total volume of hydrogen that can be economically produced. In addition, the presence of more CH_4 and N_2 in the produced gas decreases hydrogen purity, which may require additional separation or purification steps, increasing operational costs. Consequently, although CH_4 and N_2 help maintain reservoir pressure, their higher proportion diminishes the economic performance of the system, resulting in lower NPVs.

 https://doi.org/10.69631/m0g16y60

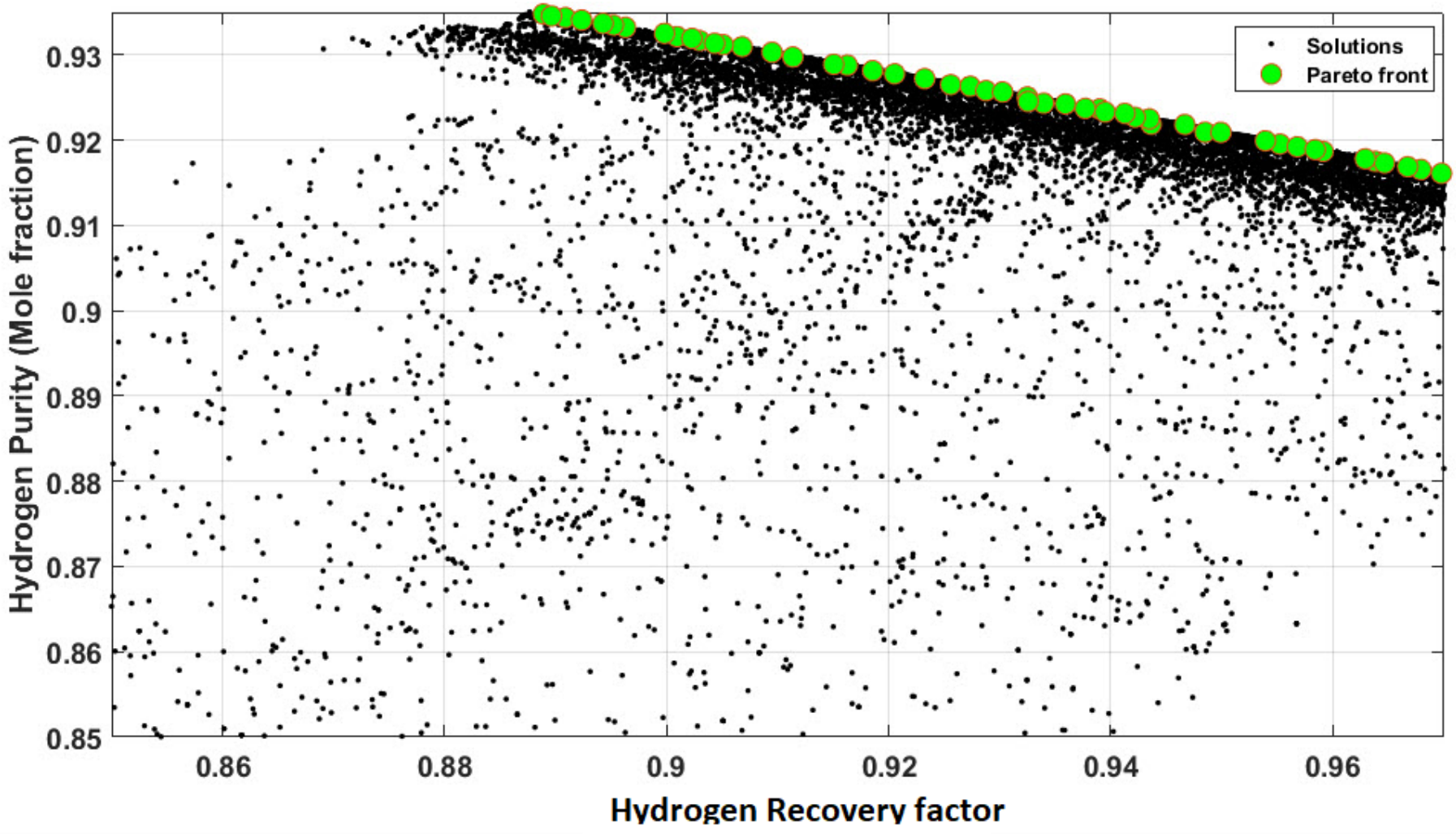

Figure 13: Pareto front of hydrogen storage optimization based on hydrogen purity and hydrogen recovery factor.

https://doi.org/10.69631/m0g16y60

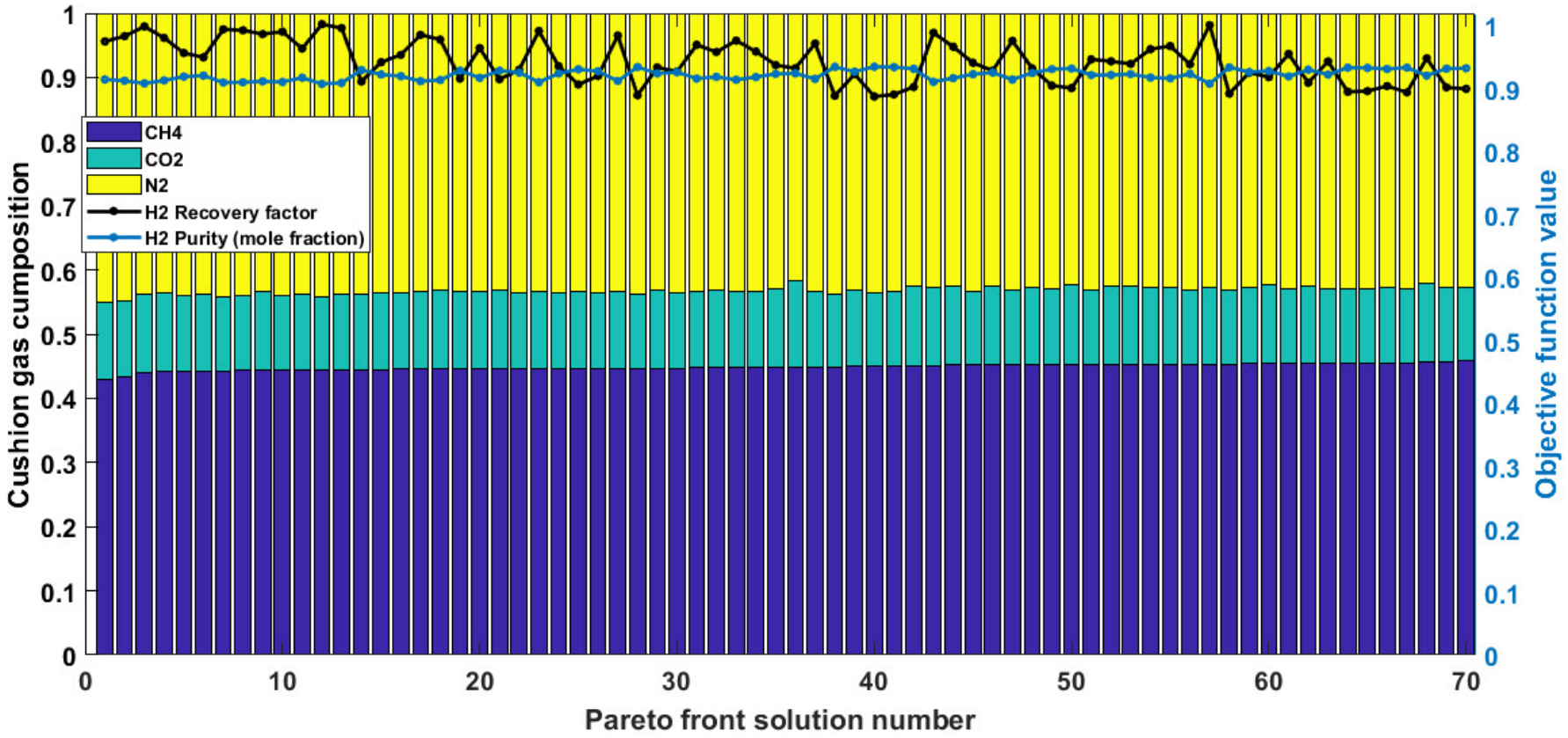

Figure 14: Optimum injected cushion gas composition based on two H_2 storage efficiency criteria.

https://doi.org/10.69631/m0g16y60

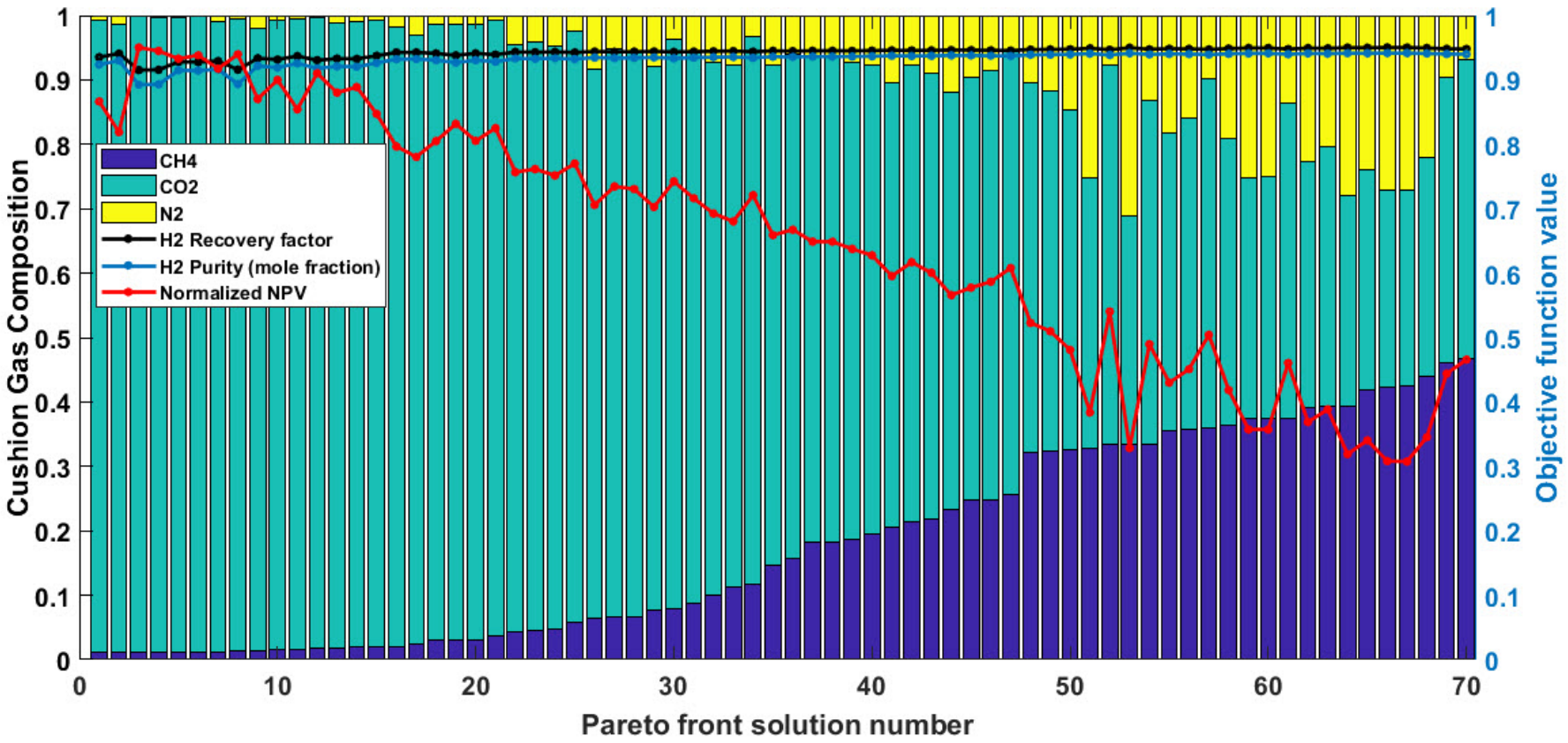

Figure 15: Optimum injected cushion gas composition based on three H_2 storage efficiency criteria.

https://doi.org/10.69631/m0g16y60

Table 6: Statistical summary of the top ten optimum solutions based on hydrogen recovery factor.

	Decision variables						**Objective function**	
	q_{ci}	q_i	q_p	y_{CH4}	y_{CO2}	y_{N2}	**H_2 Recovery factor**	**H_2 Purity**
Mean	3211230.9	4099635.0	4127312.3	0.4494	0.1186	0.4320	0.9565	0.7618
Median	3211177.8	4127907.1	4121801.3	0.4492	0.1180	0.4345	0.9532	0.7556
Std.	624.6	106820.6	16298.4	0.0070	0.0031	0.0063	0.0063	0.0212
Range	2336.0	305864.1	56951.6	0.0213	0.0102	0.0186	0.0163	0.0606
Min.	3209823.8	3933553.2	4114532.4	0.4393	0.1153	0.4206	0.9508	0.7384
Max.	3212159.8	4239417.3	4171484.0	0.4606	0.1255	0.4392	0.9672	0.7990

Table 5 presents the validation of the Pareto front solution with a physics-based simulation, while the well operational conditions and scenario selection using the proposed proxy model are ten times faster than the physics-based simulation (**Table 6**, **Table 7**).

Table 7: Statistical summary of the top ten optimum solutions based on hydrogen purity.

	Decision variables						**Objective function**	
	q_{ci}	q_i	q_p	y_{CH_4}	y_{CO_2}	y_{N_2}	**H_2 Recovery factor**	**H_2 Purity**
Mean	3212296.2	4392451.1	4118147.1	0.4326	0.1156	0.4518	0.6919	0.9540
Median	3212307.1	4393872.7	4116861.0	0.4316	0.1155	0.4533	0.6922	0.9544
Std.	306.0	204090.8	9125.5	0.0045	0.0009	0.0051	0.0048	0.0013
Range	1343.0	609184.6	32893.4	0.0156	0.0030	0.0180	0.0162	0.0038
Min.	3211601.1	4086205.7	4109844.9	0.4276	0.1141	0.4397	0.6852	0.9520
Max.	3212944.2	4695390.4	4142738.3	0.4432	0.1171	0.4578	0.7014	0.9558

4. CONCLUSIONS

This systematic study was conducted to explore the potential of intelligent, computationally efficient proxy models as an alternative to conventional physics-based reservoir simulations for UHS. The primary motivation stems from the fact that full-physics compositional reservoir simulations are extremely time-consuming, particularly when performing large-scale cyclic injection and withdrawal scenario analyses under uncertainty. To address this challenge, a comprehensive set of physics-based simulations, designed using the Latin Hypercube Sampling (LHS) method, was performed in a synthetic depleted gas reservoir. The generated data bank was then employed to construct data-driven surrogate models for conducting sensitivity analysis and multi-objective optimization of operational strategies and well control conditions.

The novelty of this work lies in the integration of intelligent proxy modeling with Pareto-based evolutionary optimization utilizing NSGA-II to simultaneously maximize hydrogen recovery, hydrogen purity, and economic performance (NPV). Based on the findings of this research the following conclusions are made:

- Among different candidates for cushion gas, such as CO_2 and CH_4, pure N_2 provides high hydrogen purity because of gravity-assisted gas segregation.

 https://doi.org/10.69631/m0g16y60

- Sensitivity analysis and optimization results revealed that the best intervals for injection are bottom perforations, and for production are top perforations, because of the gravity overrise of hydrogen in the reservoir.
- The feed-forward ANN model-with test accuracy equal to R^2 values of 0.9465, 0.9868, and 0.9995- serves as a reliable data-driven surrogate model (ten times faster) for predicting UHS performance metrics (e.g., hydrogen purity, recovery factor and NPV) in multi-objective optimization using the evolutionary NSGA-II algorithm. Overall, given the high accuracy and efficiency of the surrogate model, which significantly reduces computational effort while maintaining robustness and reliability, it is recommended for application in real-field production optimization and future well placement studies.
- The Pareto front analysis revealed that the optimal composition of cushion gas for UHS consists of 45% N_2, 40% CO_2, and 15% CH_4, which ensures operational efficiency of storage. However, from both economic and operational efficiency consideration 100% CO_2 is the optimal solution.
- Furthermore, the operational strategy of seven months of injection followed by five months of production was identified as the best performing scenario.

The methodologies followed in this research and the findings are significant for UHS management and they provide guidelines for selecting the most effective cushion gas mixture and operational schedule, thereby improving storage capacity, minimizing losses, and enhancing H_2 recovery efficiency. However, as with most data-driven and AI-based studies, the developed surrogate models primarily learn the underlying patterns within the range of the available training data and therefore are expected to provide reliable interpolation for scenarios similar to those studied, while their extrapolation capability to fundamentally different reservoir conditions remain limited. Hence, future research is recommended to address some of the limitations of this study, and to account for reservoir heterogeneity, hysteresis, and other physicochemical effects of hydrogen storage.

STATEMENTS AND DECLARATIONS

Supplementary Material

Supplementary Material for this paper is available online.

Acknowledgements

Financial support from Sharif University of Technology (Grant No. G4000103) is gratefully acknowledged.

Author Contributions

H. Kheirollahi: Data curation, Investigation, Methodology, Formal analysis, Software, Validation, Visualization, Writing (original draft, review & editing). **S. Ayatollahi:** Conceptualization, Formal analysis, Methodology, Resources, Supervision, Validation, Writing (review & editing). **H. Mahani:** Conceptualization, Methodology, Formal analysis, Resources, Supervision, Validation, Writing (review & editing).

Conflicts of Interest

The authors declare that they have no known competing financial interests or personal relationships that could have appeared to influence the work reported in this paper.

Data, Code & Protocol Availability

Data can be made available upon reasonable request.

ORCID IDs

Hossein Kheirollahi https://orcid.org/0009-0006-7534-992X
Shahab Ayatollahi https://orcid.org/0000-0001-7561-6393
Hassan Mahani https://orcid.org/0000-0002-3157-7991

Nomenclature	
CAPEX	Capital Expenditure
DOE	Design of Experiment
PMs	Proxy models
RF	Recovery factor
N_{co}	Courant number
NPV	Net Present Value
NSGA-II	Non-dominated sorting Genetics Algorithms
Q_j	Quantity of j^{th} item in objective function
U_j	Unit value of j^{th} item in objective function
D_{num}	Numerical Dispersion
f	Conversion factor
k	trade off value
i	Discount rate
n_w	Corey's exponent for water
n_{H2}	Corey's exponent for Hydrogen
Kr_w^*	End point relative permeability for water
Kr_w^*	End point relative permeability for Hydrogen
q_c	Cushion gas injection rate
q_i	working gas injection rate
q_p	Production gas rate
Ω_a, Ω_b	Peng-Robinson equation of state parameters
t	time
μ	Arithmetic Mean
σ	Standard deviation
ζ_i^+, ζ_i^-	Slack variables
ε	Half of deviation

REFERENCES

1. Alavala, C. R. (2008). *Fuzzy logic and neural networks: Basic concepts & application* (1st ed). New Age International (P) Ltd., Publishers.
2. Asghari, M., Emami Niri, M., & Sedaee, B. (2025). UHSNet: Deep learning-based smart proxy modeling for underground hydrogen storage. *Energy*, *329*, 136763. https://doi.org/10.1016/j.energy.2025.136763
3. Atrbarmohammadi, S., Kheirollahi, H., Ayatollahi, S., & Pishvaie, S. (2025). Utilizing machine learning classification models for acid–oil emulsion prediction in laboratory acidizing static tests using a hybrid databank. *Journal of Petroleum Research*, *34*(6), 73–91.
4. Bahrami, M., Izadi Amiri, E., Zivar, D., Ayatollahi, S., & Mahani, H. (2023). Challenges in the simulation of underground hydrogen storage: A review of relative permeability and hysteresis in hydrogen-water system. *Journal of Energy Storage*, *73*, 108886. https://doi.org/10.1016/j.est.2023.108886
5. Bahrami, P., Sahari Moghaddam, F., & James, L. A. (2022). A review of proxy modeling highlighting applications for reservoir engineering. *Energies*, *15*(14), 5247. https://doi.org/10.3390/en15145247

6. Eltahan, E., Albadan, D. J., Delshad, M., Sepehrnoori, K., & Alpak, F. O. (2024). Optimizing hydrogen storage in the subsurface using a reservoir-simulation-based and deep-learning-accelerated optimization method. *SPE Annual Technical Conference and Exhibition*, D021S028R002. https://doi.org/10.2118/220865-MS
7. Esfandi, T., Noruzi, Y., Safavi, M. S., & Sadeghnejad, S. (2025). Analyzing key parameters in underground hydrogen storage using machine learning surrogate models. In J. Yao, Y. Yang, W. Wang, H. Sun, L. Zhang, & K. Zhang (Eds.), *Progress and Challenge of Porous Media: Proceedings of the 16th Annual Meeting Conference on Porous Media* (pp. 978–986). Springer Nature Singapore. https://doi.org/10.1007/978-981-96-2983-1_83
8. Eslami Nia, M., Maleki Asl, P., Mahani, H., & Ayatollahi, S. (2025). Techno-economic feasibility of underground hydrogen storage in Iran: A path to sustainable energy integration. *International Journal of Energy and Water Resources*, *9*(4), 1767–1778. https://doi.org/10.1007/s42108-025-00350-2
9. Fu, S., Mao, S., Carbonero, A., Srikishan, B., Creasy, N., Chellal, H., & Mehana, M. (2025). Deep learning-based surrogate modeling for underground hydrogen storage. *Advances in Water Resources*, *203*, 105014. https://doi.org/10.1016/j.advwatres.2025.105014
10. Han, Z., Tariq, Z., & Yan, B. (2025). A novel robust optimization framework based on surrogate modeling for underground hydrogen storage in depleted natural gas reservoirs. *InterPore Journal*, *2*(3), IPJ250825-6. https://doi.org/10.69631/ipj.v2i3nr69
11. He, Q., Mohaghegh, S. D., & Liu, Z. (2016). Reservoir simulation using smart proxy in SACROC unit—Case study. *SPE Eastern Regional Meeting*, SPE-184069-MS. https://doi.org/10.2118/184069-MS
12. Juez-Larré, J., Gonçalves Machado, C., Yousefi, H., Wang, T.-K., Groenenberg, R., & Van Gessel, S. (2023, May 15). *(Pre)Feasibility study of underground hydrogen storage potential in depleted gas fields and salt caverns in the Netherlands*. https://doi.org/10.5194/egusphere-egu23-10005
13. Kanaani, M., Sedaee, B., Asadian-Pakfar, M., Gilavand, M., & Almahmoudi, Z. (2023). Development of multi-objective co-optimization framework for underground hydrogen storage and carbon dioxide storage using machine learning algorithms. *Journal of Cleaner Production*, *386*, 135785. https://doi.org/10.1016/j.jclepro.2022.135785
14. Kheirollahi, H., Zayedi, M., Sobhani, S., Chahardowli, M., & Simjoo, M. (2023). Using an ensembled artificial intelligence approach for EOR methods screening in oil fields. *Petroleum Research*, *33*(1402–5), 51–62.
15. Le Duigou, A., Bader, A.-G., Lanoix, J.-C., & Nadau, L. (2017). Relevance and costs of large scale underground hydrogen storage in France. *International Journal of Hydrogen Energy*, *42*(36), 22987–23003. https://doi.org/10.1016/j.ijhydene.2017.06.239
16. Li, Y., & Nghiem, L. X. (1986). Phase equilibria of oil, gas and water/brine mixtures from a cubic equation of state and henry's law. *The Canadian Journal of Chemical Engineering*, *64*(3), 486–496. https://doi.org/10.1002/cjce.5450640319
17. Malki, M. L., Chen, B., Mao, S., Chen, F., & Mehana, M. (2024). OPERATE–H_2: A tool for optimizing underground hydrogen storage. *Journal of Energy Storage*, *90*, 111715. https://doi.org/10.1016/j.est.2024.111715
18. Mao, S., Chen, B., Malki, M., Chen, F., Morales, M., Ma, Z., & Mehana, M. (2024). Efficient prediction of hydrogen storage performance in depleted gas reservoirs using machine learning. *Applied Energy*, *361*, 122914. https://doi.org/10.1016/j.apenergy.2024.122914
19. Matthew, D. A. M., Jahanbani Ghahfarokhi, A., Ng, C. S. W., & Nait Amar, M. (2023). Proxy model development for the optimization of water alternating CO_2 gas for enhanced oil recovery. *Energies*, *16*(8), 3337. https://doi.org/10.3390/en16083337
20. Nazari, F., Farajzadeh, R., Shokri, J., Vahabzadeh, E., Lopez-Porfiri, P., Perez-Page, M., & Niasar, V. (2025). Implications of non-ideal gas dispersion for underground hydrogen storage. *Chemical Engineering Journal*, *507*, 160143. https://doi.org/10.1016/j.cej.2025.160143
21. Ng, C. S. W., Jahanbani Ghahfarokhi, A., Nait Amar, M., & Torsæter, O. (2021). Smart proxy modeling of a fractured reservoir model for production optimization: Implementation of metaheuristic algorithm and probabilistic application. *Natural Resources Research*, *30*(3), 2431–2462. https://doi.org/10.1007/s11053-021-09844-2
22. Omeke, J., Misra, S., & Retnanto, A. (2024). Rapid forecasting of underground hydrogen storage using Fourier-integrated hybrid neural framework. *ADIPEC*, D031S088R005. https://doi.org/10.2118/222738-MS

23. Peaceman, D. W. (2010). *Fundamentals of numerical reservoir simulation*. Elsevier Scientific Pub. Co.
24. Pérez-Vigueras, M., Sotelo-Boyás, R., González-Huerta, R. D. G., & Bañuelos-Ruedas, F. (2023). Feasibility analysis of green hydrogen production from oceanic energy. *Heliyon*, *9*(9), e20046. https://doi.org/10.1016/j.heliyon.2023.e20046
25. Risso, F. V. A., Risso, F. F., & Schiozer, D. J. (2008). Risk assessment of oil fields using proxy models: A case study. *Journal of Canadian Petroleum Technology*, *47*(08). https://doi.org/10.2118/08-08-09-TN
26. Schuetter, J., Mishra, K. S., Ganesh, P. R., & Mooney, D. (2014). Building statistical proxy models for CO_2 geologic sequestration. *Energy Procedia*, *63*, 3702–3714. https://doi.org/10.1016/j.egypro.2014.11.399
27. Vapnik, V. N. (1995). *The nature of statistical learning theory*. Springer New York. https://doi.org/10.1007/978-1-4757-2440-0
28. Vaziri, P., & Sedaee, B. (2024). An application of a genetic algorithm in co-optimization of geological CO_2 storage based on artificial neural networks. *Clean Energy*, *8*(1), 111–125. https://doi.org/10.1093/ce/zkad077
29. Yan, H., Zhang, W., Kang, J., & Yuan, T. (2023). The necessity and feasibility of hydrogen storage for large-scale, long-term energy storage in the new power system in China. *Energies*, *16*(13), 4837. https://doi.org/10.3390/en16134837
30. Zhao, Y., Wei, Y., Zhang, S., Guo, Y., & Sun, H. (2024). Multi-objective robust optimization of integrated energy system with hydrogen energy storage. *Energies*, *17*(5), 1132. https://doi.org/10.3390/en17051132
31. Zhou, Z.-H. (2012). *Ensemble methods: Foundations and algorithms* (1st ed.). Chapman and Hall/CRC. https://doi.org/10.1201/b12207